Sciencia Acta Xaveriana
An International Science Journal
ISSN. 0976-1152

Volume 6
No. 2
pp. 1-48
September 2015

Introduction to Molecule based Nano magnetic Materials

Tulika Gupta

Dept. of Chemistry, IIT Bombay, Mumbai-400076

Abstract: "Molecular Magnets are single molecules consisting of a magnetic core and shielding organic ligands. "Molecular Magnets with versatile dimensionality, whether they are zero-dimensional single-molecule magnets (SMMs) or one-dimensional single-chain magnets (SCMs) have wide potential applications as they permit investigation of the fundamental aspects lying at the interphase of quantum and classical physics at the nanoscale level. This area has been such extensively explored in the quest of procuring a solid being magnetically ordered at long distance without interaction between molecules. This is viable due to the concomitant anisotropic barrier, which resulted in proper alignment of molecule in a given direction and is of purely molecular origin. Once directed in a direction, the magnetization of the molecular solid relaxes very slowly either by thermal action, above the barrier, or by "tunnelling effect" through the anisotropic barrier. This is another of the wonders of quantum mechanics, to be able to cross obstacles without having to jump them. They have magnetic anisotropy and show ferromagnetic behavior when cooled sufficiently. This makes them interesting not only for data storage purpose but also for observing quantum effects in mesoscopic objects. The ferromagnetic behavior is due to the high spin ground state and its (2S+1) secondary spin states. Because of the negative Zero Field Splitting an energy barrier is created that causes the magnetization to relax slowly over time because the thermal inversion of the magnetic moment is phonon induced with steps of $\Delta M_S = -1$ or $\Delta M_S = -2$. Additionally Quantum Tunneling of Magnetization, appearing at degenerate states, enhances the relaxation process. The contribution of this phenomenon increases with increasing temperature. SMMs open a new way towards high density magnetic information storage; it indeed becomes possible to dream of anisotropic molecular systems with high spin, assembled from the bottom or "bottom up" from small molecular precursors,on which it would be possible to store information on a single molecule.The challenge is formidable but gives a remarkable field for synthetic chemists, quantum physicists and engineers to work together in

synergy. To finally use Molecular Magnets as Bits in a binary System an implementation to a medium is required. In this talk the implementation to Carbon Nanotubes is addressed."

Motivation and Basic Knowledge: The idea of storing information using the ferromagnetic property of a remanent field goes back to 1898 where Valdemar Poulsen, a Danish Engineer, invented the Telegraphon. This device was capable of storing a magnetic amplitude which was proportional to the recorded signal on a moving wire. The principle had not changed when Fritz Pfleumer, a German-Austrian engineer, upgraded the recording medium to a tape which carried a powder of iron oxide. The obvious benefit of the new medium was the low weight and the increased capacity. He granted his idea to the German company AEG which built the worlds first tape recorder named Magnetophon K1. A real revolution had taken place when IBM 1956 invented the first magnetic hard drive, the IBM 305, which could store the amount of 5 MB of data with a density of 2000 b/in^2. In the following years improvements have been made to increase the density of hard drives exponentially (doubling every two years) to the current value of 300 Gb/in^2. This increase will find its limit because of the superparamagnetic limit. This phenomenon refers to thermally induced spin flipping at sufficiently low temperatures.

Acknowledgement: This review is written partly based on Diamond Jubilee celebration lecture at the department Chemistry, St. Xavier's College, Tirunelveli, Tamilnadu by Prof. Gopalan Rajaraman, Department of Chemistry, IIT Bombay and also based on his lecture notes on Advances in Molecular magnetism at the department of Chemistry, IIT Bombay. We would like to express our gratitude to all the eminent scientists across the world working in the area of molecular magnetism since past two decades, i.e. Prof. O. Kahn, Prof. D.Gatteschi, Prof. R. Sessoli, Prof. A. Caneschi, Prof. A.K.Powell, Prof. J. Long, Dr. J. V. Slageren, Prof. M. Murugesu, Prof. R.E.P.Winpenny, Prof. L. Chibotaru, Prof. J. Tang, Dr. L. Ungur, Prof. W. Wernsdorfer, Prof. G. Christou, Prof. E. K. Brechin, Prof. L .Jones, Prof. E. Coronado, Prof. E. Colacio, Prof. E. Ruiz, Prof. K. S. Murray, Prof. N. Ishikawa, Prof. Helene Bolvin, Prof. E. J. McInnes, Prof. D. Collison, Prof. R. Clerac, Prof. C. Coulon, Prof. A. Bencini, Prof. L. Bogani, Prof. S. Piligkos, Prof. M. Evangilisti, Prof. M. Affronte, Prof. G. Aromin, Prof. K. Bernot, Prof. V. Chandrasekhar, Prof. A. Duncan, Prof. F. Neese, Prof. H. Miyasaka, Dr. S. Langley,J. Friedman, Prof. K. Dietrich and Prof. S. Maheswaran. Most importantly, we are indebted to Prof. M. Verdaguer whose lectures on molecular magnetism have been used for our summarised write-up on molecular magnetism. We have also taken suggestions from books written by Prof. O. Kahn, Prof. E. J. Miller and M. Drillon, Prof. E. K. Itoh and M. Kinoshita, Prof. M. Verdaguer and Prof. E. Linrt proved to be extremely beneficial for our summary. We have performed thorough study on all of their published materials on molecular magnets and procured ideas have been used to write this journal and perform calculations for our research project. Eventually, GR would like to acknowledge financial support from the Government of India through the Department of Science and Technology (SR/NM/NS-1119/2011) and Indian Institute of Technology, Bombay to access the high performance computing facility. TG would like to thank UGC New Delhi for SRF fellowship.

§1. Molecule based magnets and Molecular NanoMagnets:

We consider an assembly of magnetic molecules interacting ferromagnetically, and we assume that these molecules are all of the same type. At temperatures much higher than T_c intermolecular interactions do not influence the magnetic properties. If each molecule contains a unique magnetic center, then the magnetic susceptibility χ varies according to the Curie law, provided that there is no first-order orbital momentum. If each molecule contains several magnetic centers, the intramolecular interactions generally predominate. These may be either FM or AFM, but, in this latter case, they must lead to a nondiamagnetic ground state. Such a situation is achieved, for instance, for an odd number of equivalent local spins, or for a pair of nonequivalent local spins. If we ignore intermolecular interactions for a moment, then the molar magnetic susceptibility χ should follow the Curie law in the temperature range where only the molecular ground state is thermally populated, with the Curie constant depending on the ground state spin. Actually, we assume that significant intermolecular ferromagnetic effects are operative. If this is so, as T decreases and approaches T_c, χ increases faster than anticipated for the Curie law, which is easily detected when plotting χT versus T. χT increases more and more rapidly on cooling. This enhancement in χT is related to an increase in the correlation length. At temperatures not too close to T_c the intermolecular interactions can be fairly well accounted for by the mean-field approximation. At T_c, χ and χT should in principle diverge, and a spontaneous magnetization should appear. On cooling further, the magnetization increases to a saturation value $Ms = N\beta gS$, where S is the spin associated with the molecular ground state and g is the Zeeman factor.

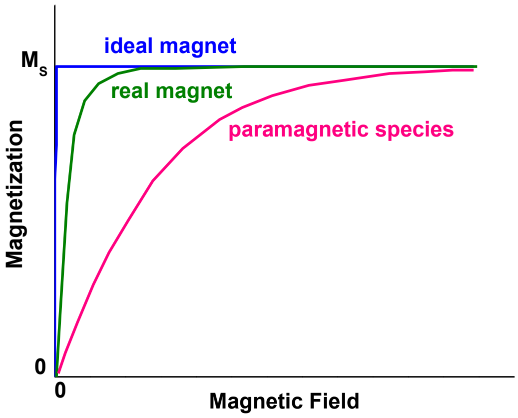

Figure 1.Magnetization vs magnetic field plot for different kind of magnetic species

Practically at zero magnetic field, no magnetization is usually detected. This is governed by two factors, domain formation and demagnetizing field. A sample of a ferromagnetic material is generally broken into domains. Each domain has a net magnetization in zero field, directed in a given direction. The magnetic moments of the domains are randomly oriented within the sample such that the resulting magnetization is zero. An external magnetic field provokes a displacement of the domain walls and the formation of a new domain structure. The magnetic moments of the domains are no longer randomly oriented but tend to align along the field. A magnetization M is then observed. If the sample was a monodomain, the M = f{H) variation at T≤ Tc would be as shown in below figure with an infinite zero-field susceptibility $(dM/dH)_{H=0}$. Since domain formation is taking place, the slope of the M versus H plot for H = 0 is very large but not infinite. We need to emphasise that increase of M vs H is much faster for a ferromagnetic material than for a paramagnetic system.

However, if the ferromagnetic and paramagnetic samples contain the same spin carriers, then the saturation magnetizations are identical; this saturation will be reached for a much lower field in ferromagnetic samples than in paramagnetic samples (see Figure 1). The other factor that limits the zero-field susceptibility, the demagnetizing field, is due to uncompensated moments at the surface of the sample, in the opposite direction to that of the magnetization of this sample. This demagnetizing field can be measured in principle if we have the idea of the geometry of the sample. All our aforementioned basic about molecule based magnets have neglected anisotropic effects owing to spin orbit coupling. These effects are speculated to be negligibly small for purely organic materials, the magnetic properties of which are associated with s or p electrons. EPR spectroscopy of organic radicals clearly exhibits that the orbital contribution is extremely weak. The resonance is always observed for g-values very close to $g_e = 2.0023$. On the other hand, magnetic anisotropy may be important for metal ion-containing compounds. It leads to a preferred spin orientation, called an easy magnetization axis. For $T \leq Tc$, the zero-field susceptibility $(dM/dH)_{H=0}$ is larger and the saturation magnetization Ms is reached at a weaker field when this field is applied along the easy magnetization axis.

There is another aspect that is quite typical of ferromagnetic materials, including the molecular-based ferromagnets, namely, remnance and hysteresis. When the magnetic field is switched on below Tc, then switched off, the field-induced magnetization does not totally disappear, which is in contrast with what happens for paramagnetic systems. In some cases, this remnant magnetization may be equal to the field-induced magnetization. All the information is retained. To suppress the remnant magnetization, it is necessary to apply a coercive field in the opposite direction. Remnant magnetization and coercive field define the hysteresis loop and confer a memory effect to the material. The mechanism of the hysteresis phenomenon is discussed before. Hysteresis takes much more time for the magnetic moments of the ferromagnetic domains to reorient randomly when the field is switched off than for those of paramagnetic molecules. Molecular magnetism was initiated at the NATO advanced study institute, ASI, held in Castiglion della Pescaia in Italy in 1983(Willet et. Al. 1983). [8]The title of the ASI, ‘Structural–magnetic correlations in exchange coupled systems’, reflects the interest of the chemist organizers for understanding the conditions under which pairs of transition metal ions could give rise to ferromagnetic interactions. Looking at the list of participants it is clear that there was a blend of chemists and physicists, many of whom met for the first time. A common language started to be developed and useful collaborations were established for the first time. The proceedings of that ASI have been intensively referenced, and have been the textbook for the first generation of scientists active in molecular magnetism.

Synthesising and designing bulk magnets originating from molecules always remain cumbersome due to difficulties in organising 3D net of strong magnetic interactions. Scenario becomes easier with ions or metals, where the building block are spherical, while reality remains always far with the building blocks, being of low symmetry. This enables the easy procurement of comparatively large number of low-dimensional materials using molecular building blocks.

However, this difficulty may turn out to be an advantage if the target is changed from three-dimensional magnets to low-dimensional and, in particular, zero-dimensional magnets. Indeed the interest in finite-size magnetic particles had developed in the 1980s as a consequence of the growing interest in the so-called nanoscience. It was realized that nanosize objects can be particularly interesting because matter organized on this scale has enough complexity to give rise to new types of properties, and yet it is not too complex and can be investigated in depth in much detail. The interest in nanoscience (and, in perspective, for nanotechnology) spans all the traditional disciplines. conductors and semiconductors, as a result of the impetus on the miniaturization processes associated with more efficient computers. One of the challenges is the realization of objects of size so small that they gave rise to the coexistence of classical and quantum properties. The most interesting results were in the field of quantum dots and quantum wires , [9, 10] which correspond to objects whose size is in the nanometre range in three or two directions, respectively. Progress was made possible by the development of experimental techniques, which allowed 'seeing' and investigating the properties of particles of a few nanometres. Among them a particular relevant place was kept by scanning probe microscopy techniques, like atomic force microscopy, scanning tunnel microscopy, etc.

Magnetism could not be an exception, and one of the relevant themes was the possibility of observing quantum tunnelling effects in mesoscopic matter. A scheme, showing the size effects in the magnetization dynamics and hysteresis loop going from multidomain magnetic particles to molecular clusters has been given below as suggested by Sir Wernsdorfer in 2001.

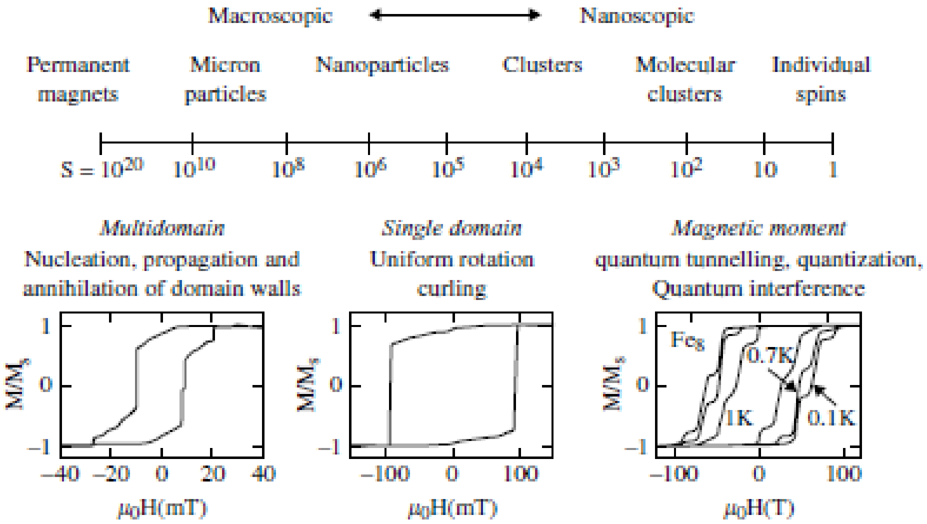

Figure 2. The above figure shows transition from macroscopic to nanoscopic magnets. The hysteresis loops are typical example of magnetization reversal via nucleation, propagation, annihilation of domain walls (left), via uniform rotation (middle) and quantum tunnelling (right). [11]

At the macroscopic limit the particles contain at least billions of individual spins, which are coupled in such a way that the individual moments will respond all together to external stimuli. The magnetic energy is minimized by forming domains, regions in space within which all the individual moments are parallel (antiparallel) to each other. The orientation of the moments of the domains will be random in such a way that in the absence of an external magnetic field the magnetization of the sample is zero. The transition from a domain to the neighbouring one will occur through a region where the local magnetic moments are rapidly varying, called the Bloch walls. The width of the Bloch walls, d, depends on the exchange coupling constant *J*, which tens to keep the spins ordered and to make the walls as large as possible, in order to minimize the effort needed to change the orientation of the moments, and on the magnetic anisotropy, which tends to minimize the Bloch walls to reduce the probability of high-energy orientations. Obviously the width of the domain walls depends on the nature of the magnetic material.

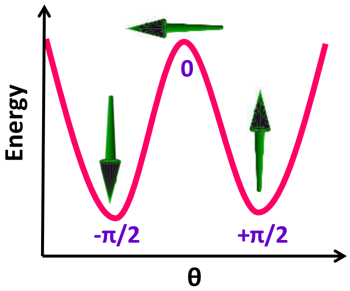

Figure 3. Plot of energy of an Ising (easy axis) type magnet as a function of the angle of the magnetization from easy axis.

When the sample is magnetized all the individual moments will eventually be parallel to each other and the magnetization reaches its saturation value. If the field is decreased the formation of domains will not be reversible in such a way that the magnetization at zero field will not be zero, like in the non-magnetized case. The finite value of the magnetization in zero field is called the remnant magnetization. In order to demagnetize the sample it is necessary to go to a negative field, which is called the coercitive field. This value is used in order to classify the bulk magnets: a small value of the coercitive field is typical of soft magnets, while in hard magnets the coercitive field is large. The M/H plot, shown in above figure on the left, shows a hysteresis loop, which tells us that the value of the magnetization of the sample depends on its history. This is the basis of the use of magnets for storing information.

On reducing the size of the magnetic particles a limit is reached when the radius of the particle is small compared to the Bloch wall depth. Energetically the process of domain wall formation is no longer economical and the particle goes single domain.

By further reducing the size of the particles, another effect is further invoked. The magnetic anisotropy of the sample, A, depends on the size of the particle:

$$A = KV$$

V is the volume of the particle and K is the anisotropy constant of the material. Let us suppose that the anisotropy of the magnetization is of the Ising type, i.e. the stable orientation of the magnetic moment of the particle is parallel to a given direction z. The energy of the system as a function of the orientation of the magnetic moment is pictorially shown in beside figure. This figure represents energy of an Ising (Easy axis) type magnet as a function of the angle of the magnetization from easy axis. In the figure The bottom of the left well corresponds to magnetization down, the bottom of the right well to magnetization up, and the top to the magnetization at 90° from the easy axis. On reducing the size of the sample eventually the barrier for the reorientation of the magnetization will become comparable to the thermal energy. If the sample is prepared with the magnetization up (right well) some of the particles will have enough energy to jump over the barrier and reverse their magnetization. If the particles are given enough time, half of them will be in the left and half in the right well at equilibrium because the two minima have the same energy. The system will no longer be magnetized in zero magnetic field, like a paramagnet. If an external field is applied then one of the two wells will lower its energy and the other will increase it. The two wells will have different populations and the system behaves like a paramagnet, but since the response to the external perturbation comes from all the individual magnetic centres, it will be large. These kinds of particles are called superparamagnets, and they find some interesting application, like in magnetic drug delivery, in magnetic separation of cells, and as a contrast agent for magnetic resonance imaging.

An important feature of the superparamagnet is that the observation of either static or dynamic magnetic behaviour depends on the time-scale of the experiment used for investigating it. For instance, using an ac magnetic susceptibility measurement with a field oscillating at ν =100 Hz, static behaviour, with a blocked magnetization, will be observed if the characteristic time required for the particles to go over the barrier is longer than $\tau = (2\pi\nu)^{-1}$, while dynamic behaviour is observed for shorter τ . The so-called blocking temperature (T_B) corresponds to the temperature at which the relaxation time of the magnetization equals the characteristic time of the experiment.

The characteristic time for the reorientation of the magnetization can be easily calculated assuming that it occurs through a thermally activated process. This gives rise to an exponential dependence on the energy barrier with so-called Arrhenius behaviour, as observed in many other classes of thermally activated physical and chemical processes:

$$\tau = \tau_0 \exp \frac{KV}{K_B T}$$

This behaviour is typical of a classical system. In principle, when the size of the magnetic particles reduces, it may be possible to invert the magnetization also through the quantum tunnel effect. [12] This effect should show up at low temperature, where it should provide the most efficient path for magnetic relaxation only if the wavefunctions of the left and of the right well have some overlap. The quest for exploring quantum effects in magnetic nanoparticles will be investigated in detail.

The size of the particles needed to observe superparamagnetic behaviour ranges from 2–3 to 20–30 nm, depending on the nature of the material. Magnetic nanoparticles are obtained in many different ways, ranging from mechanical grinding to sol–gel techniques. An original procedure uses naturally occurring materials like ferritin, the ubiquitous iron storage protein. Iron is needed in the metabolism of living organisms, and it must be stored in some place in order to use when it is needed. Nature chose ferritin to do this job in animals, plants, fungi, and bacteria. Man has an average of 3–4 g iron and ca. 30 mg per day are exchanged in plasma. Structurally ferritin comprises a proteic shell, apoferritin, and a mineral core, of approximate composition FeOOH. The size of the internal core is ca. 7 nm, giving rise to superparamagnetic behaviour in the iron oxide particles, which can contain up to ca. 4000 metal ions.

Definite improvements have been made recently in the techniques to obtain monodisperse assemblies of magnetic particles. In some cases it has been possible to obtain identical particles that have been ‘crystallized’.In fact if spherical particles all identical to each other are put together they will try to occupy space in the most efficient way, giving rise to a close packed array exactly as atoms do in crystals.

An alternative to using magnetic nanoparticles, i.e. of reducing the size of bulk magnets in a sort of top-down approach, is that of using a molecular approach in a bottom-up approach. [13] The idea is that of synthesizing molecules containing an increasing number of magnetic centres. In the ideal process one would like to be able to add one magnetic centre at a time, starting from one and going up to say a few thousand magnetic centres. The theoretical advantage of the molecular approach is that molecules are all identical to each other, therefore allowing the performance of relatively easy experiments on large assemblies of identical particles, and still being able to monitor elusive quantum effects. Molecules can be easily organized into single crystals, therefore allowing the performance of accurate measurements. Further, they can be investigated in solutions, thus destroying all the intermolecular magnetic interactions that might give rise to spurious effects. As an alternative to single crystals it is possible to organize them in self-assembled monolayers and address them with microscopic techniques like STM. Therefore molecular nanomagnets have great promise and they well deserve the effort needed to design and synthesize them.

The idea of making molecules of increasing size by adding the magnetic centres one at a time is certainly appealing, but unfortunately it is not like that that chemistry goes. However, some successful strategies have led to noticeable results such as the spectacular increase in the size of manganese molecular clusters achieved by Christou and co-workers and schematized in following figure 4:

Hence, magnetic molecular clusters which are known as molecular nanomagnets have received this classification due to their presence at the final point in the series of smaller and smaller units from bulk matter to atoms. To date they have been the most promising candidates for observing quantum phenomena as they have a well defined structure with well characterized spin ground state and magnetic anisotropy. Moreover, they can be regularly assembled in large crystals where all molecules often have the same orientation. Therefore, macroscopic measurements can give direct access to single molecule properties.Hence, molecular nanomagnets can be referred to as large (Avogadro's) number of magnetic molecules which are nearly identical, providing ideal laboratories for the study of nanoscale magnetic phenomena. Hence, Molecular nanomagnets have been undergoing development for 20 years since the first single-molecule magnet (SMM), Mn$_1$2Ac,[16] was characterized as the molecule-behaved magnet. The multi-disciplinary scientists promoted the magnetic characteristics to be more suitable for use in information science and spintronics.[17] The concept of molecular nanomagnets has also evolved to include single-chain magnets (SCMs), single-ion magnets (SIMs) and even magnetic molecules that showed only slow magnetic relaxation, in addition to the initial cluster-type SMMs. The discovery and subsequent development of molecular nanomagnets (single-molecule magnets, SMMs; single- chain magnets, SCMs; single-ion magnets, SIMs) have led to a fascinating intermediate regime between the realm of paramagnetism and bulk magnetism. Below the so-called blocking temperature T_B, the magnetization reversal of a molecular nanomagnet is efficiently blocked owing to an effective energy

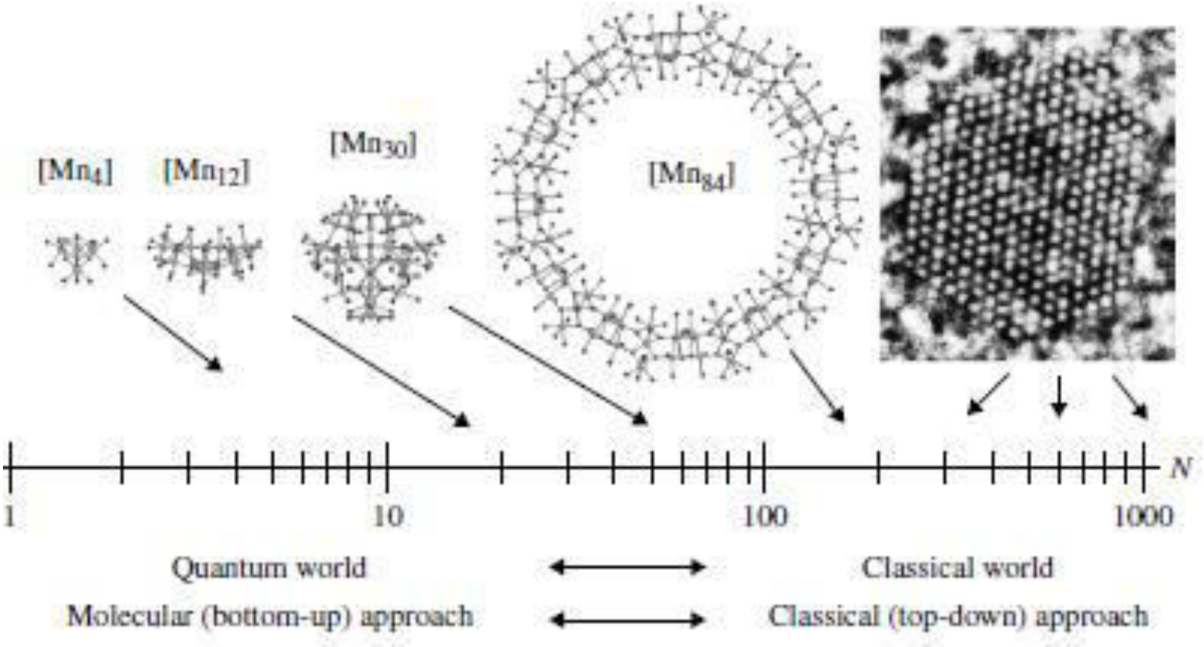

Figure 4. Increasing size and nuclearity of molecular clusters containing manganese ions that approach the size of nanosized magnetic particles.[14, 15]

barrier U_{eff}, and magnetic hysteresis of purely molecular origin can be observed. Furthermore, quantum properties, such as quantum tunnelling of the magnetization and quantum interference, were observed in these systems, leading to the potential applications of molecular nanomagnets in molecule spintronics, spin valves, transistors and the future generation of information storage and quantum computing.

§1.1. Representative examples of Single Molecule Magnets (SMMs) and mononuclear SMMs or Single Ion Magnets (SIMs):

§16.1.1.Characteristics:

Hence, single molecule magnets (SMMs) could retain magnetisation in the absence of a magnetic field. They Represent the smallest possible magnetic storage device, retaining information in a single molecule rather than in a magnetic particle or an array of particles. SMMs undergo quantum tunnelling and are possible q-bits in quantum computers. "*A single molecule that behaves as a nanoscale magnet below a critical temperature. i.e. displays hysteresis of molecular origin".*

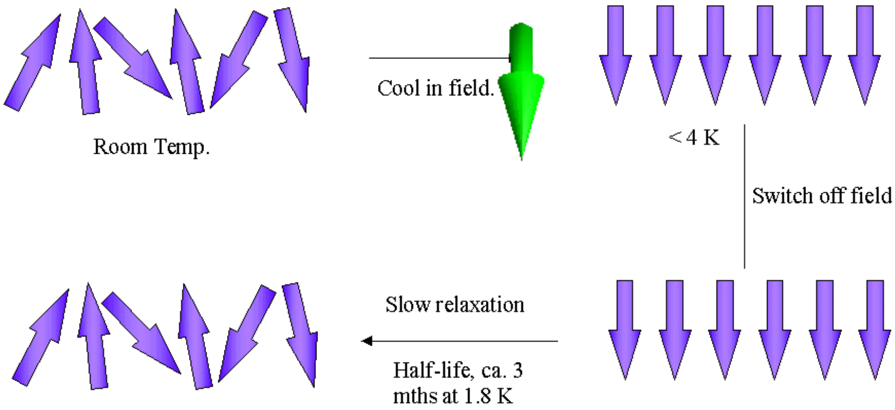

Figure 5. Pictorial representation of the orientation of electronic spins of a single molecule magnet.

Hence, a SMM can be regarded as a molecule which exhibits slow relaxation of magnetization of purely molecular origin. It is molecule which will be magnetized in presence of magnetic field and even will retain its magnetization on removal of the field. This feature is solely molecular characteristics and no intermolecular interactions are needed to spur such phenomenon. This differentiates SMMs from its traditional bulk magnet congeners. On dissolving a SMM in a solvent or placing into some matrix (i.e. polymer) we will be able to detect SMM property. SMMs are basically general class of complexes i.e. exchange coupled clusters. Most often, SMMs are parts of a mineral lattice encapsulated by the organic ligands. In materials sciences, one molecule of SMM can be considered as one bit which led to unprecedented data densities almost reaching the superparamagentic limit. SMMs are class of compounds which fall between classical and quantum magnetic systems and distinctly exhibit quantum properties. The properties of molecular magnets are usually illustrated in the spin Hamiltonian model (as discussed before in section 15.2). The large ground spin state (S) of a molecule can be determined by exact diagonalization using irreducible tensor methodology. This S ground state possesses 2S+1 spin microstates which will correspond to the m_S state in the absence of transverse anisotropy. These states can be subsequently splitted in zero-field induced by spin orbit coupling or magnetodipolar interactions give S>1/2(zero-field splitting, discussed before in detail). Magnitude of magetodipolar interactions are generally negligible (10^{-1} cm^{-1}) but solely originates zero-field splitting for organic radicals. The orbital angular momentum of the electronic ground state is supposedly quenched by spin0orbit coupling and Jahn-Teller distortion. Spin orbit coupling can mix the orbital angular momentum of the electronically excited state into the ground state. Zero-field splitting can also be expressed with spin Hamiltonian which includes D(axial zfs; changes the energies of the M_S states, but not the characters) and E(rhombic/transverse zfs; mixes the M_S states and varies the characters of the microstates). Based on the aforementioned points, we can plot the energies of the microstates against M_S or against the angle of the magnetic moment with the quantization axis. Within the energy potential wall (shown in figure 6), the splitted 21 microstates can undergo phonon induced transition amongst them in compliance with the selection rule of $\Delta M_S=1$ or $\Delta M_S=2$. This gives rise to an energy barrier towards thermal inversion of the magnetic moment. Todate very few experimental techniques are viable in detecting zero field splitting i.e. High Filed Electron Paramagnetic Resonance (HFEPR), Inelastic Neutron Scattering (INS) and Frequency Domain Magnetic Resonance (FDMRS). This necessitates the use of sophisticated tool in order to gain deeper insights into the zfs property of a SMM. In absence of any magnetic field, the energy levels on the left and right sides of the potential energy double well in the energy barrier diagram (shown in figure 6 and 7) are degenerate. In absence of transverse anisotropy source is distortion along the XY plane), the energy eigenstates are the pure M_S states(as shown in Figure 6 left picture).

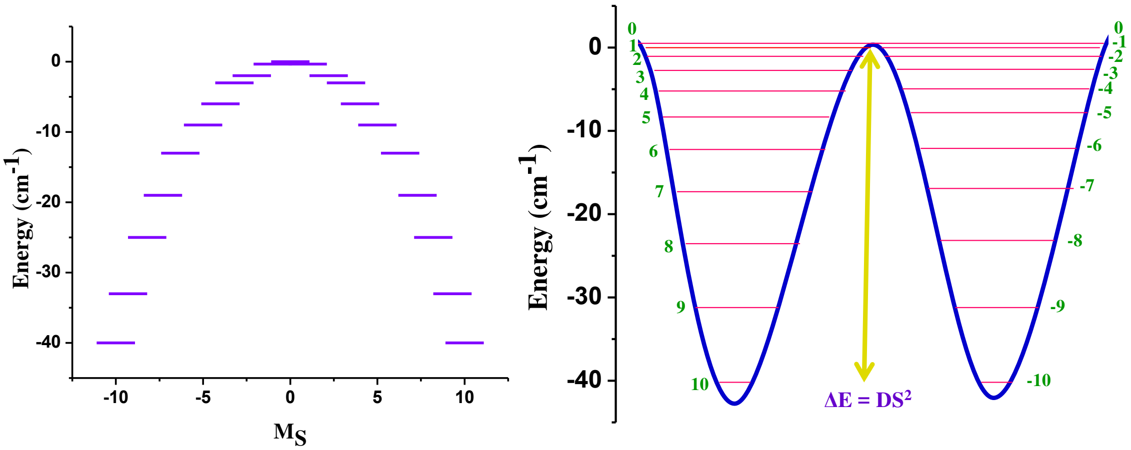

Figure 6. Splitting of the S=10 level into its 21 M_S microstates are plotted with respect to their corresponding energies and the angle of the magnetic moment of the quantization axis as well.

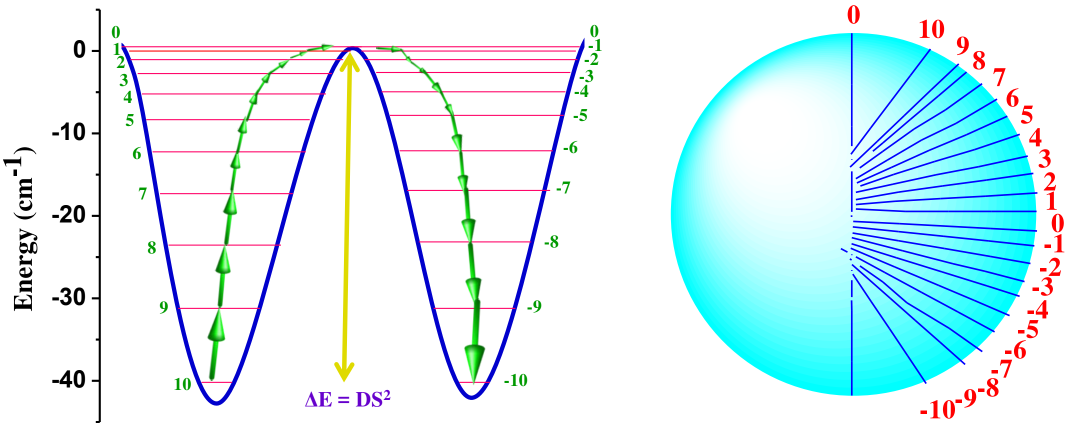

Figure 7. Diagram showing magnetic relaxation in a complex with S=10 ground state represented by electron (electronic spin expressed by green arrows) from $M_S=+10$ level tends to relax back to the equilibrium state of $M_S=-10$ level. We have also shown the consecutive splitting of the S=10 level into its 21 M_S microstates.

On introduction of transverse anisotropy, the M_S microstates no longer remain energy eigenstates. Near the bottom-line of the potential energy barrier wall, eigenstates become the superposition of the M_S states on the left and right side of the potential energy double wall. At the upper portion i.e. higher energy levels, the second order transverse anisotropy mixes M_S levels with $\Delta M_S=2$, and the fourth order transverse anisotropy those with $\Delta M_S=4$. Overall, the eigenstate now can be considered as $|M_S\rangle+|-M_S\rangle$ and $|M_S\rangle-|M_S\rangle$ and splitting between these two admixtured states are termed as tunnel splitting (Δ). From static point of view, we can comment that, the system is located both on the left and right side of the energy barrier while from dynamic overview, the system oscillates coherently between the two sides of the potential energy double wall at a frequency equal to the tunnel splitting, until magnetic coupling to the environment destroys coherence. Generally, tunnel splitting in SMMs is very small and magnetization can tunnel but only coherently.

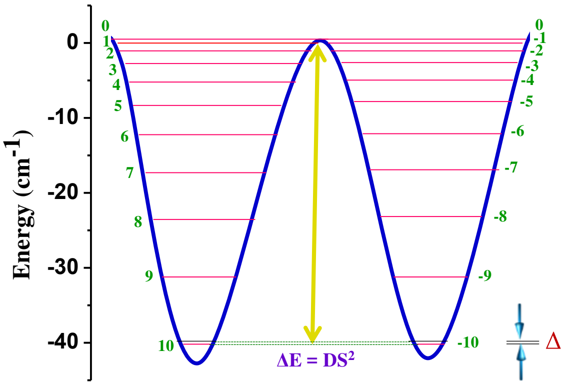

Figure 8. Potential energy double wall showing superposition of the ± M_S with the identification of tunnel splitting (Δ).

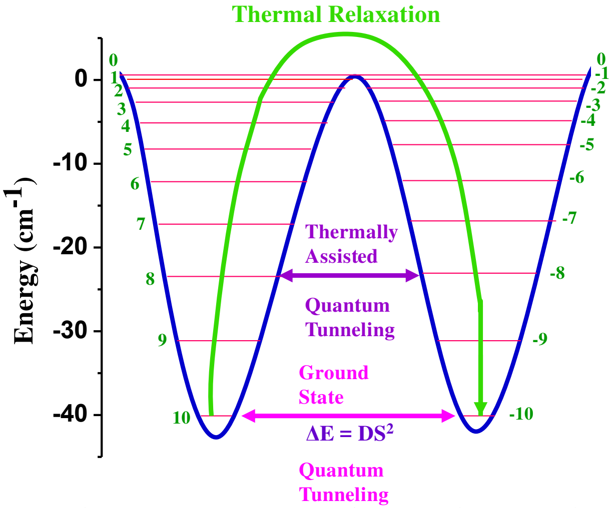

Figure 9. Occurence of magnetic relaxation via three different pathways: (i) thermal relaxation (ii) thermally assisted quantum tunnelling (TA-QTM) and (ii) ground state quantum tunnelling (QTM).

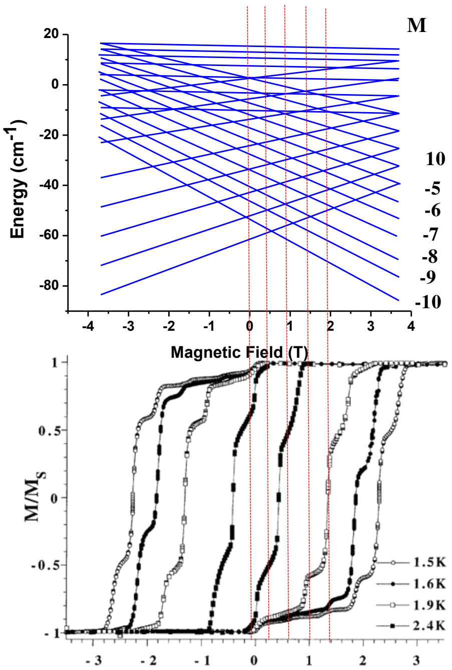

Figure 10. Splitting into the ± M_S correlates to the magnetic hysteresis curve.[4]

On application of longitudinal magnetic field, the spin microstates change energy according to the Zeeman interaction which leads to the crossing of the microstates at certain levels. At these fields transverse anisotropy mixes the $\pm M_S$ levels enabling the tunnelling of magnetization (QTM). The two $\pm M_S$ levels of double wall are degenerate or in resonance with respect to each other in absence of magnetic field(Figure 11).

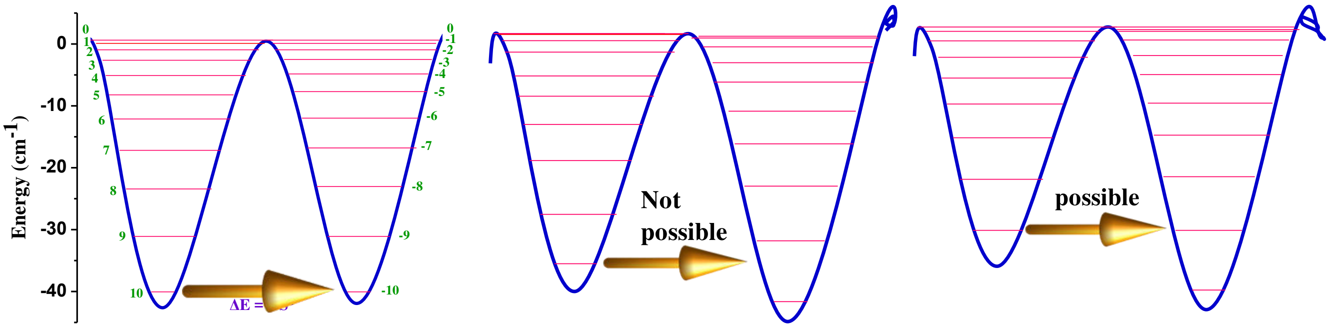

(a) (b) (c)

Figure 11. Three different possible shapes of the double well potential are (a) Showing transition/QTM between the ground state degenerate $\pm \mathbf{M_S}$ levels. (b) no ground state transition possible between non-degenerate energy levels. (c) On relocating the ground state $\pm M_S$ levels , again the QTM becomes a possible pathway.

It is worthwhile to mention that, magnetism detected in a single molecule differes in its source as compared to the origin of classical magnetism. SMMs are nanoclusters in which molecular unit may possess several paramagnetic ions/electronic spins. A SMM contains substantial potential energy barrier for reorientation of the magnetization direction. If the magnetic moments of individual molecules in a crystal of a SMM are oriented in parallel direction, the temperature is reduced, the magnetic field is removed, the SMM would remain magnetized along with the parallel spins at low temperatures. The prerequisite to exhibit SMM characteristics are to have large ground spin state (S) and appreciable amount of magnetic anisotropy (zero-field splitting). To be an active SMM, a molecule has to show relaxation of magnetization below c characteristic blocking temperature (T_B) which originates from large spin ground state (S, large number of unpaired electrons) in combination with the presence of large,negative Ising (easy axis) type of magnetic anisotropy(zfs,D) whose cut-off values are being provided by $S^2|D|$ or $(S^2-1/4)$ $|D|$ for integer and half-integer spins respectively.

The slow relaxation of magnetization in SMMs arise basically due to the presence of an energy barrier in order to overcome the reversal of magnetic moment and gets backs to the equilibrium magnetization state compatible to the behaviour of super-paramagnetic materials.

Super-paramagnetic behaviour takes place when a single magnetically ordered domain possesses reorientation barrier compatible to the thermal energy. This enables free magnetization flipping, property similar to that observed in a paramagnet. In presence of external magnetic field, this behaves like a a paramagnet till the temperature is sufficiently decreased such that the energy barrier cannot be easily dealt with. Hence, blocking of magnetization takes place below a blocking temperature (T_B), and the super-paramagnet reverts back to its usual bulk behaviour (ferro/antiferro/ferri magnetic materials).As mentioned before that, axial anisotropy(D) enforces magnetic moment alignment in either parallel(spin-up) or antiparallel(spin-down) alignment with respect to the quantization (easy) axis.,energy barrier for the magnetization reversal or energy needed to reorient the magnetization to its equilibrium state can be represented as $S^2|D|$. For each S spin state, 2S+1 spin projections or energy states have been procured. In the absence of any transverse anisotropies or field, energy states with equal bur opposite spin projections ($\pm M_S$) will retain degeneracy in zero magnetic field. The energy eigenvalues for each eigenstate can be described as, $E(m_s) = D\ m_s^2$ (m_s is the spin projection along the z axis; the ground state for the system is the greatest magnitude of the spin projection ($m_s = \pm S$), since D is negative. The axial anisotropy defines a quantization axis (z axis in general), for the energy levels for the system, which are quantized. The energy barrier creates the bistable magnetic state owing to energetic preferential orientation in +z direction or antiparallel in –z direction.

In absence of any magnetic field, anisotropy gets introduced within a system which also brings forth zero-field splitting parameter. However, in presence of external magnetic field Zeeman interaction is manifested within the molecule in terms of magnetic anisotropy. In an external magnetic field, the Zeeman energy of an electron relies on the alignment of the magnetic field with respect to the spin projection along the magnetic field. The energy of the Zeeman interaction is correlated to the strength of the external magnetic field through a proportionality factor. Zeeman energy depends upon Bohr magneton, external magnetic field strength, Lande factor, and spin operator of the molecule. Zero-field anisotropy has profound impact on magnetic properties and magnetic hardness is correlated to the magnetoanisotropy. Qualities of a super-paramagnet is seen within an SMM which also shows both frequency-dependent out-of-phase ac magnetic susceptibility(Fig 12) and hysteresis in a graph of magnetization vs applied dc magnetic field which are characteristics of magnetic materials.

AC susceptibility studies reveal that at several oscillation frequencies can be utilised in order to determine the true effective energy barrier for magnetization relaxation (U_{eff}) as at the χ_m'' peak maximum magnetization relaxation rate ($1/\tau$, where τ is the relaxation time) equals to the angular frequency ($2\pi\nu$) of the oscillating field. Hence, out-of-phase ac measurements at various oscillation frequencies are a variable source of relaxation rate vs T kinetic data that can be fitted to the Arrhenius equation:

$$1/\tau = (1/\tau_0) \exp(-U_{eff}/KT) \qquad \text{and} \qquad \ln(1/\tau) = \ln(1/\tau_0) - U_{eff}/KT$$

The relaxation time in an SMM is expected to follow the Arrhenius equation (as shown by straight line in the adjacent figure 13). Besides showing the aforementioned classical properties, SMMs also show quantum properties i,e, quantum tunnelling of magnetization (QTM) through the energy barrier.

Magnetic hysteresis is one another unique property associated with SMMs, observed at low temperature so that each molecule behaves as a tiny magnet. This leads to the observation of “steps” in the hysteresis loop and imply the presence of quantum mechanical “short-cuts” for the reversal of the magnetic moment. Such steps clearly reveal the presence of QTM, and take place only when the m_S levels on each side of the potential energy double well become degenerate resulting from the applied magnetic field which further induces tunnelling of the magentization vector. So, as discussed before, QTM can be described as the tunnelling of the magnetization vector from a energy level on one side of the classical energy barrier to the energy state on the other side. Phonon assisted QTM occurs on excitation of the magnetization vector to higher energy m_s levels which subsequently tunnels through the energy barrier.

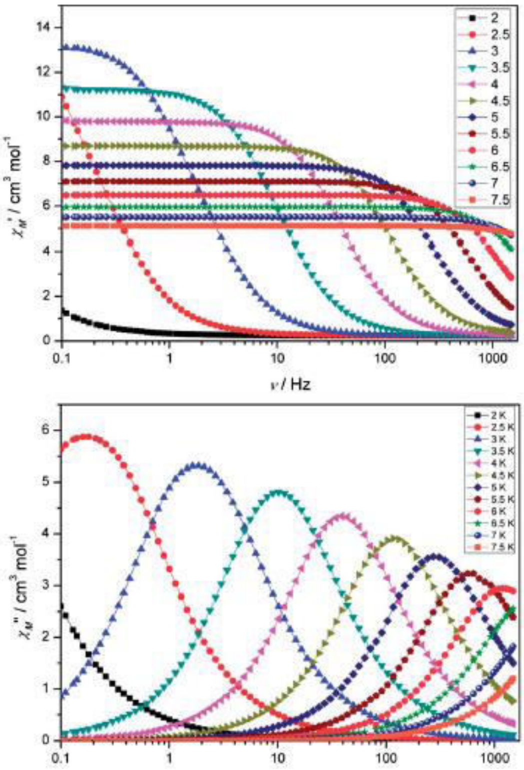

Figure 12. In-phase and out-of-phase AC magnetic susceptibility of $[Cr^{III}_2Dy^{III}_2(OMe)_2(bdea)_2(acac)_4(NO_3)_2]$ [6]

Hence, we can say that increasing the S and D will instill the quest of obtaining improved SMMs. While, increasing S value proportionate the enhancement of the number of unpaired electrons which requires vigorous experimental endeavour and to some extent cumbersome also. Hence, the focus of obtaining better SMMs have been diverted towards the synthesis of complexes possessing metal ion with large magnetic anisotropy. Complexes possessing single metal ion with large magnetic anisotropy have been proved their ability to show excellent energy barrier for magnetization reversal and increased blocking temperature.[18 5 19 20 21 22, 23 24 25 26, 27]

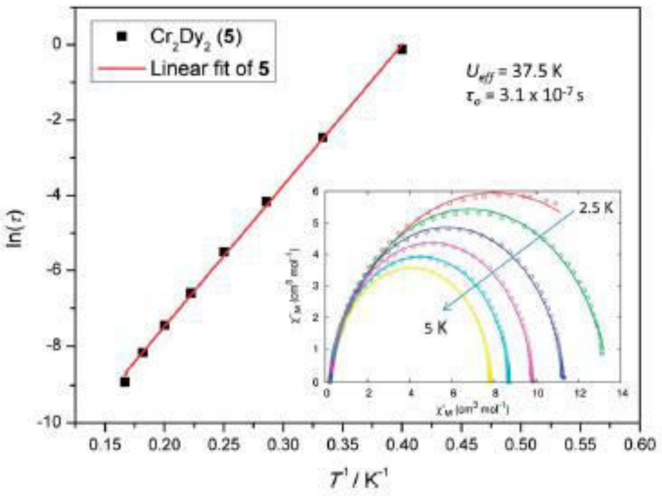

Figure 13. Plot of the natural logarithm of the magnetization relaxation rate vs 1/T for $[Cr^{III}_2Dy^{III}_2(OMe)_2(bdea)_2(acac)_4(NO_3)_2]$ [6]

The anisotropy barrier can be determined from magnetic susceptibility measurements in a a very small dynamic or alternating current (ac) magnetic field, which can be undertaken either in zero static direct current (dc) field or in an applied dc field. During the performance of such experiments, in-phase (χ’) and out-of-phase (χ'') components of the magnetic susceptibility are measured as a function of the variable ac frequency (ν). The χ'' vs ν plot enables the estimation of relaxation time τ from $\tau = 1/2\pi\nu$, ν is the peak maximum (figure 13; inset). The relaxation dynamics are expressed by a relaxation time τ at a particular temperature and frequency which further permits determination of the anisotropy barrier from the equation $\ln(1/\tau) = \ln(1/\tau_0) - U_{eff}/KT$. The U_{eff} values can be extracted from the linear section of the ln τ vs 1/T plot, this depicts a regime where relaxation is thermally activated.

Measure of the success of an SMM is whether or not the field dependence of the magnetization shows hysteresis. If a molecule is indeed "magnetic", then, after being subjected to a reverse magnetic field (H) and subsequently returned to zero-field conditions, it will display nonzero magnetization (M). This phenomenon is also temperature dependent; however, other factors such as the field sweep rate determine the maximum temperature (the blocking temperature, T_B) at which M(H) hysteresis is observed. It is possible to compare SMMs characterized using different sweep rates by defining the blocking temperature as the temperature at which the magnetic relaxation time is 100 s. Many SMMs show M(H) hysteresis; however, all current examples require liquid helium cooling, and one of the major challenges is to raise the blocking temperature to levels that will be more convenient for the development of device applications. Hence, recent extensive research on SMMs have been undergoing towards achieving high temperature single molecule magnets. [28]

. §1.1.2.detailed analysis of the properties of first ever discovered mn12ac molecule:

The first SMM was discovered in a coordination complex made of 12 oxide and acetate bridged manganese ions, with formula $[Mn_{12}O_{12}(O_2CMe)_{16}(H_2O)_4](Mn_{12}Ac)$ have received appreciable attention due to its unusually large magnetic moment and magnetic bistability. This complex shows large S=10 ground state, and associated with large negative magnetocrystalline anisotropy barrier of 70K which has resulted a characteristic relaxation time and magnetic hysteresis below a blocking temperature (T_B) of 3K. The magnetic core of Mn_{12}-ac has four Mn^{4+} (S=3/2) ions in a central tetrahedron surrounded by eight Mn^{3+} (S=2) ions. The ions are coupled by superexchange through oxygen bridges with the net result that the four inner and eight outer ions point in opposite directions, yielding a total spin = 10.

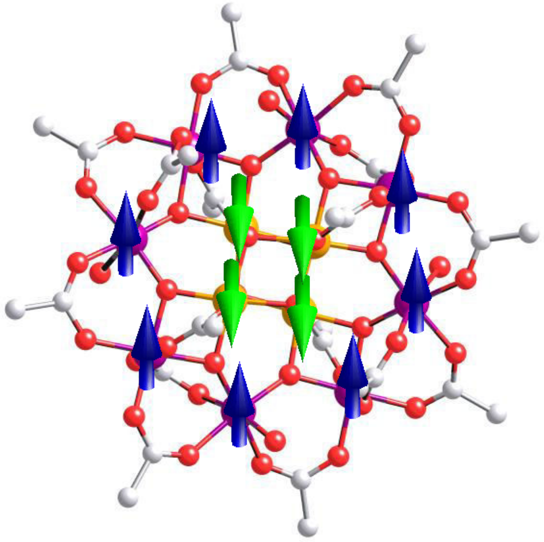

Figure 14. Crystal structure of first ever invented SMM $[Mn_{12}O_{12}(O_2CMe)_{16}(H_2O)_4]$

The magnetic core is surrounded by acetate ligands, which serves to isolate each core from its neighbors, and the molecules crystallize into a body-centered tetragonal lattice. Whereas there are very weak exchange interactions between molecules, the exchange between ions within the magnetic core is very strong, resulting in a rigid spin(-10) object that has no internal degrees of freedom at low temperatures. The large spin ground state arises from antiferromagnetic interactions between the S =3/2 spins of Mn^{IV} ions and the S =2 spins of Mn^{III} ions, which do not compensate. A strong uniaxial anisotropy barrier of the order of 70 K yields doubly degenerate ground states in zero field. The spin has a set of levels corresponding to different projections, m = 10,9,....,-9,-10 of the total spin along the easy axis of the molecule. An axial zero-field splitting is present within the molecule which induces splitting of the S=10 state into 21 levels, each characterized by a spin projection quantum number, m_s, where $-S \leq m_s \leq S$. The above figure clearly indicates that zero field splitting (D) within the ground state leads to an energy barrier (E_a). Each level has an energy given as $E_a(m_s) = m_s^2D$ {D= axial zero-field splitting parameter and m_s=magnetic spin quantum number}, where for the $Mn_{12}Ac$ molecule shows axial zero-field splitting parameter D of -0.50 cm^{-1}.This negative sign of D leads to a potential energy barrier

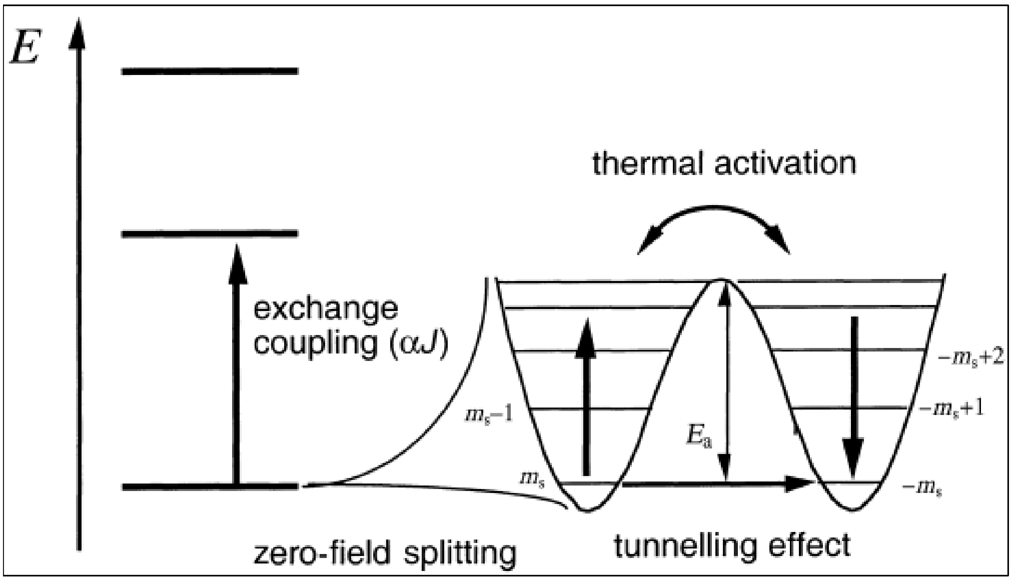

Figure 15. Diagram illustrating correlation between zero field splitting and magnetic relaxation involved in a single molecule magnet (SMM).

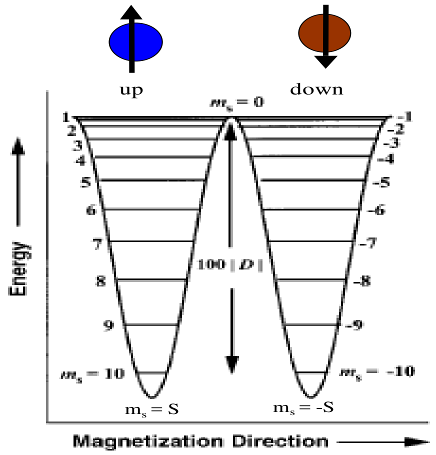

Figure 16. Splitting of S=10 level into its corresponding ± 21 m_S levels.

between the spin-up (m_s= -10) and spin-down (m_s= 10) orientations of the magnetic moment of individual $Mn_{12}Ac$ molecule. Moreover, in order to flip the spin of a Mn_{12} molecule from along the +z axis to along the -z axis of the disc-like $Mn_{12}O_{12}$ core, it takes some energy (beside figure) to reorient the spin via the perpendicular m_s=0 state. This is an easy axis type of anisotropy. If this barrier is appreciable, the spin of an SMM can be magnetized in one direction. For a thermally activated process, the time for the reorientation of the magnetization depends exponentially on the height of the barrier. $Mn_{12}Ac$ is magnetic field and then removing the field, the relaxation of the magnetization is so slow that after two months the magnetization is still about 40% of the saturation (i.e., largest) value. At 1.5 K, the half-life for magnetization decay is hardly measurable because it is too long. It has been conclusively established that the slow magnetization relaxation shown by an SMM is due to an individual molecule rather than to long range ordering as observed in nanoscale magnetic domains of bulk magnets. Support for this conclusion comes from several experiments, such as magnetization relaxation data for frozen solutions or polymer-doped samples, the absence of any anomaly in heat-capacity measurements (no long-range magnetic ordering), and high-frequency electron paramagnetic resonance (HFEPR) data.

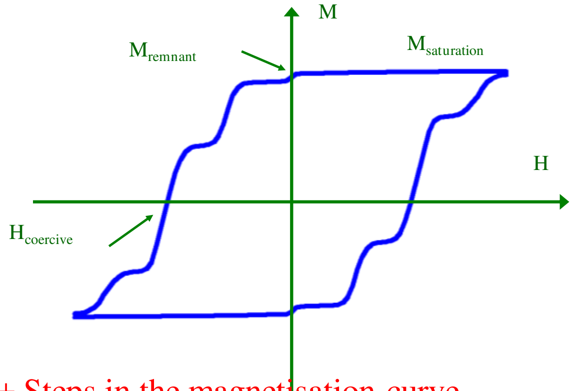

+ Steps in the magnetisation curve

Figure 17. Magnetic hysteresis and its corresponding parts.

When a sample of $Mn_{12}Ac$ molecule is exposed to a large external magnetic field, the m_s= -10 state is greatly stabilized in energy relative to the m_s= +10 state. All of the molecules have their spins aligned with the external field; all of the molecules are in the m_s = -10 state, and the magnetization is saturated. If the external field is cycled to zero, the magnetization M is frozen by the presence of the barrier and only very slowly tends to the equilibrium value (M=0). Thus, a remanent magnetization is observed. A negative field reduces the height of the barrier and unfreezes the spins, thus allowing a rapid reversal of the magnetization. A hysteresis loop is therefore observed, which has a molecular and dynamical origin. The width of the loop (i.e., the coercive field) depends on the temperature as well as the rate of sweep of the magnetic field. Large coercive fields of several Tesla have been observed for 1 below 2 K. The important feature is that at zero field, the magnetization of $Mn_{12}Ac$ can be either positive or negative, depending on the history of the sample. Therefore, it is possible in principle to

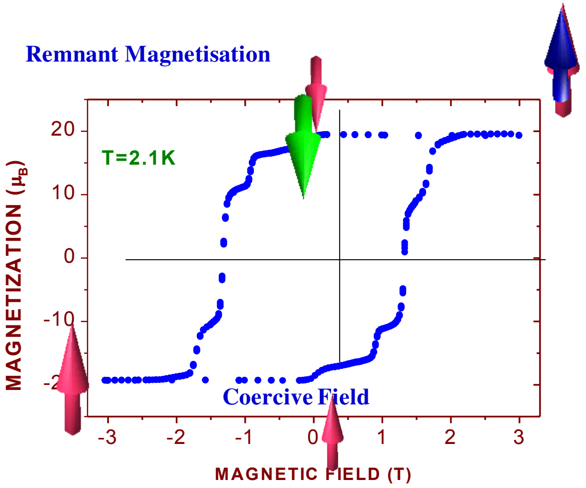

Figure 18. Magnetic bistability, hysteresis and remanent magnetization in $Mn_{12}Ac$ hard magnet.

store information in one single, bistable molecule. The magnetic anisotropy of the ground state of $Mn_{12}Ac$ largely results from the magnetic anisotropy of the eight Mn^{III} ions. The bonding at each Mn^{III} ion is such that two trans- bonds are longer than the other four (in what is called a Jahn–Teller elongation). These “crystal-field” distortions, together with a spin-orbit interaction, establish a zero-field splitting at each Mn^{III} ion. Thus, it is the vectorial projection of single-ion anisotropies onto the S = 10 ground state that gives rise to the easy axis type of magnetoanisotropy. SMMs have huge potential applications in high-density magnetic memories, magnetic refrigeration, molecular spintronics and quantum computing devices and used as multiferroic materials with magnetoelectric effect. $Mn_{12}Ac$ is a hard magnet and known for its bistability i.e. : in zero field the magnetisation can be positive or negative depending of the story of the sample. This molecule is magnetically saturated in 3T magnetic field and retains magnetization even upon removal of magnetic field. We need to apply 1T of magnetic field in order to bring back the magnetization to zero and saturation can be achieved again by application of 3T magnetic field in the downwards direction. If we switch off the magnetic field, magnetization really persists while demagnetizing the system again requires the application of substantial magnetic field. For $Mn_{12}Ac$ molecule the relaxation time at 2K is order of months and below 1.5K relaxation time is of the order of 50 years and it has application in magnetic memory devices. The steps in the curve (figure 18) indicate the occurrence of tunnelling of the electronic spins in $Mn_{12}Ac$ molecule.

Now, owing to the dependence of slow relaxation in magnetic materials on the opening of the magnetization vs field loop (hysteresis loop), gaining deeper insights into the magnetic hysteresis properties have become essential. In molecular magnets, hysteresis do not arise due to the irreversible growth of domains with the orientations of the magnetic moments parallel to the field, instead it relies on the fact that magnetization of the materials relax back at extreme slow rate compared to the time needed to sweep the field. Hence, magnetization of the magnetic material fails to reach the equilibrium value in the time-window of the experiment. Dynamics of the magnetic material solely dictates the width of the hysteresis loop. In molecular magnets, the magnetic field could have weird effect on the magnetization dynamics. This entails the accurate recording of the hysteresis loop in the exploration of the dynamics as compared to the well-known magnetic materials.

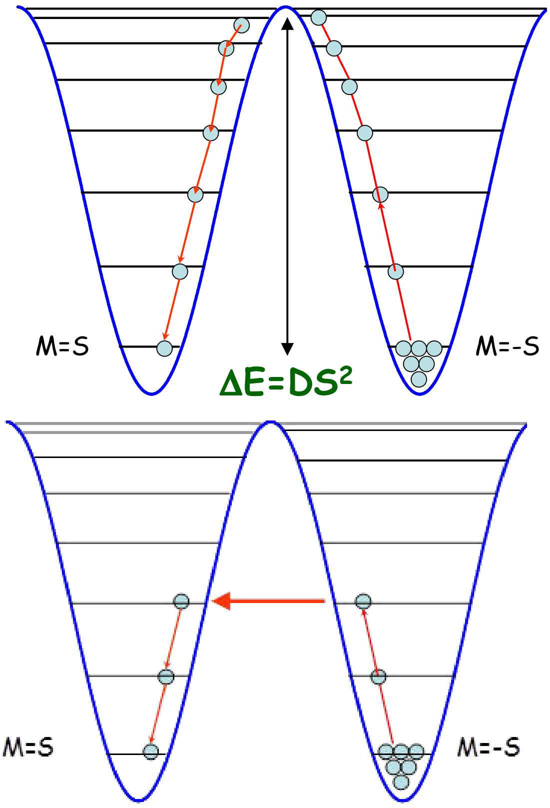

Figure 19. Top: Splitting of the S level to its Ms levels and bottom: occurrence of QTM.

Given the two ground states are degenerate, the magnetization will try to pass through the consecutive all higher energy levels in order to come back to the equilibrium state. This will be deterred if magnetization tunnel through (as shown in the Figure 152) amidst the expected energy levels which will try to cut down the energy barrier for reorientation of magnetization. Such incident is termed as quantum tunnelling of magnetization (QTM) which is induced by breakage of degeneracy of the ground state levels, perturbation of which is found to instigate QTM in the whole magnetic phenomena of a molecule. QTM equates to a loss of magnetization and is witnesses by steps in experimental loops. Admixing of degenerate states are found to induce QTM. In presence of magnetic field, the ground state levels will no longer remain degenerate (like figure 11b) and will for SMMs long time is needed to get back to the equilibrium state of magnetization.

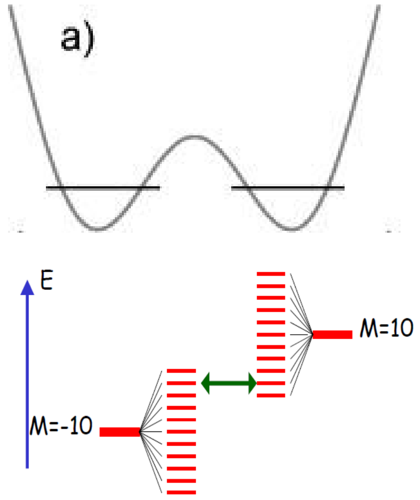

Figure 20. Top: non-interacting energy levels and bottom: non-degenerate energy states between ± M_S = 10 states.

Given the energy levels are degenerate, no interaction occurs between these levels(non-interacting state shown in figure 20,top). This interaction can be introduced by low symmetry components of the crystal field by hyperfine fields (provided by magnetic nuclei ^{55}Mn) by dipolar fields caused by neighbouring molecules. Hyperfine fields broaden the levels and are still functioning at 100 mK. To observe QTM following conditions need to be fulfilled (i) degenerated wave functions must superimpose (ii) a transversal field must couple the two wave functions (iii) coupling should split the two levels resulting tunnel splitting (iv) tunnelling effect is related to tunnel splitting and the energy barrier. Such perturbation is basically introduced by the presence of transverse anisotropy (along XY plane) basically due to deviation from the symmetry.

QTM is basically incurred onto large transverse anisotropy. For larger M_s values, smaller admixture of the two wavefunctions have resulted slowing down of the tunnelling rate. The particle oscillates

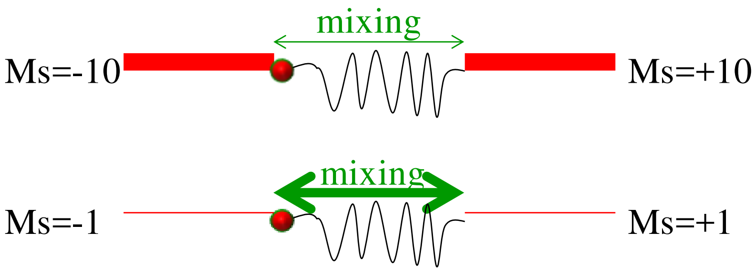

Figure 21. Admixing of the energy levels decreases between for ± M_S values.

coherently between the two sides of the potential well at a frequency equal to the tunnel splitting. In our previously discussed SMM $Mn_{12}Ac$ molecule tunnel splitting is found to be very small (in the order of 10^{-10} K).

As energy barrier for reorientation of magnetization depends on spin (S) of the ground state of the molecule and zero-field splitting (D) enhancement of both the parameters necessitates better SMM property. Increments in the number of metals do not proportionate the spin state. Instead, underlying type of magnetic interactions within the molecule determines the S value. Hence, it is necessary to arrange the metal ions and the bridging ligands in an appropriate manner in order to give rise to high spin ground state. It is worth mentioning that, large spin never always ensure an SMM with an accessible blocking temperature (T_B) due to the lack in generating large negative zero-field splitting (D) parameter. For example, Mn^{III}_6 complexes have been prepared with an S=12 ground state, but since the six Mn^{III} ions are arranged in a high-symmetry octahedron, the zero-field splitting is negligible (D=0) in these complexes. Most importantly, synthesis of complexes with large metal ions is extremely cumbersome, complicating the generation of better SMMs. It is also noteworthy that, exerting control over the symmetry of the coordination environments become increasingly difficult and elaborate/large molecular clusters tend to reduce SMM characteristics significantly. Since more than two decades, aftermath the discovery of SMMs research focus was synthesising larger clusters with the hope of obtaining better SMMs which could not be at the par with the expectations. This entails chemists and physicists to experiment with other dictating parameter (D) for energy barrier for magnetization reorientation. Hence, magnetic anisotropy is the most crucial property unifying all SMMs. The physical significance of anisotropy in SMMs is that the magnetic moment of an individual molecule has a preferred orientation, which does not depend on an external magnetic field, leading to net magnetization in a bulk sample. If the orientation of the magnetic moment is reversed - crudely, analogous to flipping spin-up to spin-down then the SMM properties are lost. In order to wipe the SMM properties in this way, a thermal energy barrier must, in principle, be surmounted: for the purposes of this review, the energy barrier is referred to as the anisotropy barrier, U_{eff}, in units of cm^{-1} (as opposed to units of K, which are also commonly used). The magnitude of the anisotropy barrier is one way of comparing the success of different SMMs, and the bigger the barrier, the larger blocking temperature, the more prominent the SMM properties at higher temperatures. Moreover, fine control over the symmetry, ligand field and nature of the ligand field is crucial in order to mitigate perturbations (QTM) and obtain improved SMMs. [29] [30-32]

§1.1.3.Transition metal based SMMs and SIMs:

Ever since the discovery of the first SMM, namely the Mn12-acetate compound, considerable efforts have been devoted to the development of this fascinating area [33, 34,35-39]aiming at the enhancement of both the T_B and U_{eff} . However, the record of the energy barrier of the SMMs was held by the first Mn_{12}-acetate compound for more than a decade until the discovery of the Mn_6 compound. Among the transition metals, at first V^{III}/V^{IV} based SMMs i.e. $[NEt_4][V^{III}_4O_2(O_2CEt)_7(pic)_2]$, $[V^{IV}_{15}As_6O_{42}(H_2O)]^{6+}$ have been observed which also incorporates polyoxometallate class of compounds. Mn containing SMMs are the most ubiquitous class amongst their other transition congeners ansd studied extensively owing to the large spin of the manganese centres in the various oxidation states, stability of the Mn complexes under aerobic conditions, the availability of many Mn complexes/salts as starting materials and ease of synthesis of these Mn containing compounds. Several Mn dimmers, tetrameric clusters have been reported as SMMs which is also corroborated by some SMMs possessing Mn metal ions. Besides these, Ni^{II}, Co^{II}, Co^{III}, Fe^{II}, Fe^{III} based SMMs have been vigorously studied in the literature. It is worth mentioning that, first row transition metal based SMMs are most ubiquitous in the literature. The first attempts to maximize the anisotropy barrier focused on maximizing S by designing systems with ferromagnetic exchange coupling. Using this approach, the largest anisotropy barrier and blocking temperature of $U_{eff} = 62$ cm^{-1} and $T_B \approx 4.5$ K, respectively, were reported for the dodecametallic phenolate-bridged cage $[Mn_6O_2(sao)_6(O_2CPh)_2(EtOH)_4]$ ({Mn_6}; $saoH_2$ = 2-hydroxybenzaldehye oxime), which was determined to have a total spin of S = 12.All these polynuclear transition metal clusters do not exhibit energy barrier according to the expectation. Moreover, difficulties in synthesis of such large clusters spur the need towards exploring other alternatives of procuring better SMMs. The first example of a monometallic 3d SMM was the high spin Fe(II) compound K[(tpaMes)Fe (H_3tpaMes = Tris((5-mesityl-1Hpyrrol- 2-yl)methyl)amine). The Fe(II) ion lies in a trigonal pyramidal geometry, with an N4 coordination sphere. The bulky ligand promotes the unusual geometry around the metal centre by impeding access to the second axial site. Owing to the anisotropy of the transition metal ion Easy synthesis of compounds containing single transition metal ion and owing to their associated magnetic anisotropy research attention has been focussed towards transition metal based Single Ion Magnets (SIMs). [40] Recent breakthrough in this field occurred with the discovery of two coordinate linear Fe(I) [41] complex $[K(crypt-222)][Fe(C(SiMe_3)_3)_2]$, which leads to large barrier height of 226 cm^{-1}. Attempts

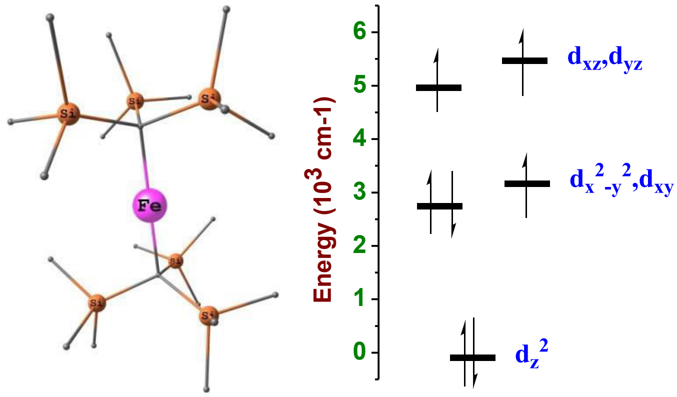

Figure 22. Crystal structure of $[Fe(C(SiMe_3)_3)_2]^-$ and energies of their 3d orbitals extracted from ab initio computed analysis

to understand the slow magnetic relaxation in Kramers ions with positive axial anisotropy have outlined the importance of physical considerations beyond the symmetry around a 3d ion, such as the importance of hyperfine interactions. Control of the relaxation pathways available to a single ion magnet should allow for improvement in performance as a potential data carrier. The physics of these compounds and how this relates to other possible applications for nanomagnets, such as quantum computing, still has wide scope for exploration. To obtain SMMs with high U_{eff} and T_B , highly Ising-type anisotropy is required for most of the time.

§1.1.4. Lanthanide based SMMs and SIMs:

Large energy barrier and blocking temperature-two important prerequisites of better SMMs are controlled by high Ising type anisotropy. This entails the inclusion of 4f metal ions which possess anisotropy alongwith unquenched orbital angular momenta and large spin orbit coupling.

Despite great synthetic efforts, the desired blocking temperatures for better SMM properties remain very low (below 4K). In this context, lanthanide ions in the periodic table are the most suitable candidates due to the associated inherent large anisotropy arising from the large unquenched orbital angular momentum, inert 4f orbitals, large magnetic moment and spin orbit coupling. They also fulfil the SMM prerequisite of possessing bistable electronic ground state and lanthanide based SMMs requisite of large m_J/ magnetic moment values. Owing to the large anisotropy, vast number of lanthanide based good SMMs have been reported in the literature since last 2-3 years. It is noteworthy that, lanthanide based SMMs have advantages in diagnostic and therapeutic radiopharmaceuticals and as luminescent probe to investigate biomedical systems. Amongst all, Dy(III) based SMMs prevail owing to the large energy gap between ground and first excited m_J levels, concomitant high magnetic anisotropy and Kramers' ion (odd number of f electrons) nature of Dy(III) [5] [1, 20, 42-46] leading to the observation of bistable ground state irrespective of the ligand field symmetry. This has resulted extensive study of several polynuclear Dy(III) based SMMs i.e. $[Dy4(\mu_3\text{-}OH)_2(\mu\text{-}OH)_2(2,2\text{-}bpt)4(NO_3)_4\text{-}(EtOH)_2]$,$[Dy_3(\mu_3\text{-}OH)_2L_3Cl(H_2O)_5]Cl_3$, $[Dy_2ovph_2Cl_2(MeOH)_3]$. $[Dy(Htea)(NO_3)]_6.8MeOH$ { Figure 23} with large energy barrier.

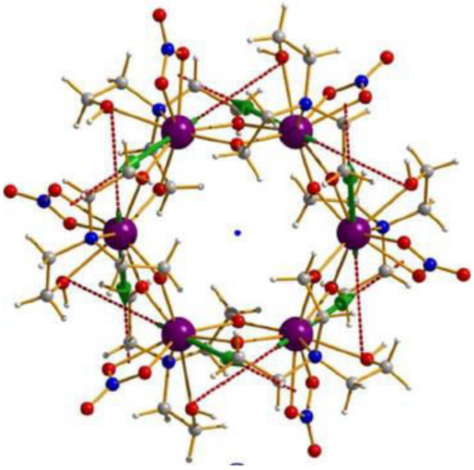

Figure 23. Crystal structure of $[Dy(Htea)(NO_3)]_6$ complex.

For lanthanide based SMMs, [47, 48] [21, 26] [49, 50] [24, 51] [52] [53-59] [60-65] [66-76] in a given crystal field, the ground magnetic state of the complex (characterized by the total angular momentum J), splits into $\pm M_J$ sublevels. In some instances, this leads to a J-splitting in which the levels with higher M_J values are stabilized with respect to the levels with lower M_J values. This leads to the appearance of a barrier between the M_J levels explaining superparamagnetic blocking in the SMMs. Of particular interest in recent years in research area of SMMs[77] is exploration of systems containing only one spin carrier within a molecule and if such molecules exhibit magnetisation blockade these are called as Single Ion Magnets (SIMs) as discussed for transition metal systems. Large unquenched orbital angular momentum, significant intrinsic spin-orbit coupling and presence of large number of unpaired electrons make the lanthanides suitable candidates for attaining large spin-reversal barriers. The early research on lanthanide SMMs can be dated back to 2003, when Ishikawa et al. demonstrated that slow relaxation of the magnetization can occur in mononuclear lanthanide species(SIMs), that is, the double-decker phthalocyanine lanthanide system $[LnPc_2]^-$ (Ln = Tb, Dy).[78, 79] Nevertheless, until 2006 the discovery of the fascinating Dy_3 triangle SMMs showing the coexistence of nonmagnetic ground states and SMM behaviour really stimulated wide interest in the exploration of pure lanthanide SMM systems with strong local Ising-type anisotropy at metal sites. Therefore, hundreds of such SMMs including mononuclear, dinuclear and larger lanthanide compounds have now been discovered to exhibit a high anisotropic barrier for reversing the magnetization and naturally some remarkable advances follow the experimental and theoretical developments in this field. However, it is worth noting that in some recently reported SMMs, the temperature dependence of τ shows obvious deviation from the Arrhenius law, and thus other processes such as Raman, direct and QTM may be added to the fitting of τ vs. T^{-1} plots. Remarkably, the highest effective barrier in multinuclear lanthanide SMM has been as high as 692 K(figure 24) which is almost comparable to the barrier record of 939 K shown by heteroleptic bis(phthalocyaninate) lanthanide SMM(figure 25).Consistent study towards obtaining better SMMs are ongoing which led to the exploration of SMMs/SIMs based on other lanthanide ions (Er,Ho,Ce).This is evidenced by possession of large 10K blocking temperature in complex $[Er(COT)_2]^-$ (see Figure 26} , zero-field SIM characteristics and large energy barrier for magnetization reorientation. Hence, advantageous properties of lanthanides

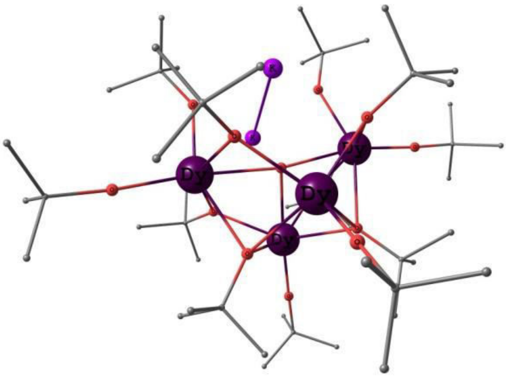

Figure 24. Crystal structure of $[Dy_4K_2O(O^tBu)_{12}]$ showing U_{eff}=692 K.[1]

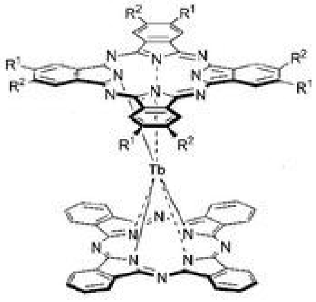

Figure 25. Crystal structure of heterpeptic $[Tb^{III}(Pc)(Pc')]$ complex in their neutral forms where $R^1=R^2=O(C_6H_4)\text{-}p^tBu$.[2]

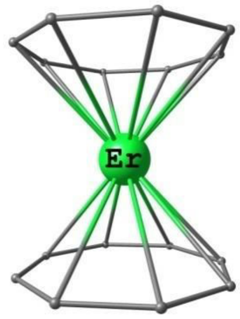

Figure 26. Crystal structure of $[Er(COT)_2]^-$ complex.[3]

require a multi- and interdisciplinary vision of scientific research by bringing together synthetic and physical chemists as well as physicists to achieve the final goal.

§ 1.1.5. Mixed SMMs:

Heterometallic complexes occupy a special place among SMMs as they offer an alternative to homometallic transition metal SMMs and often exhibit unprecedented metal topologies and beautiful structural motifs. This combinational complexes (27a) lead to new molecular species with larger magnetic anisotropies and higher S values,, the latter arising from the different nature and strength of the magnetic exchange interaction between the heterospin carriers. This class can be categorised to 3d-3d, 3d-4d,3d-5d,3d-4f, 4f-4f and only 4f ion based complexes[5, 25, 26, 42, 51, 52, 62, 79-94],4f-2p type of complexes.

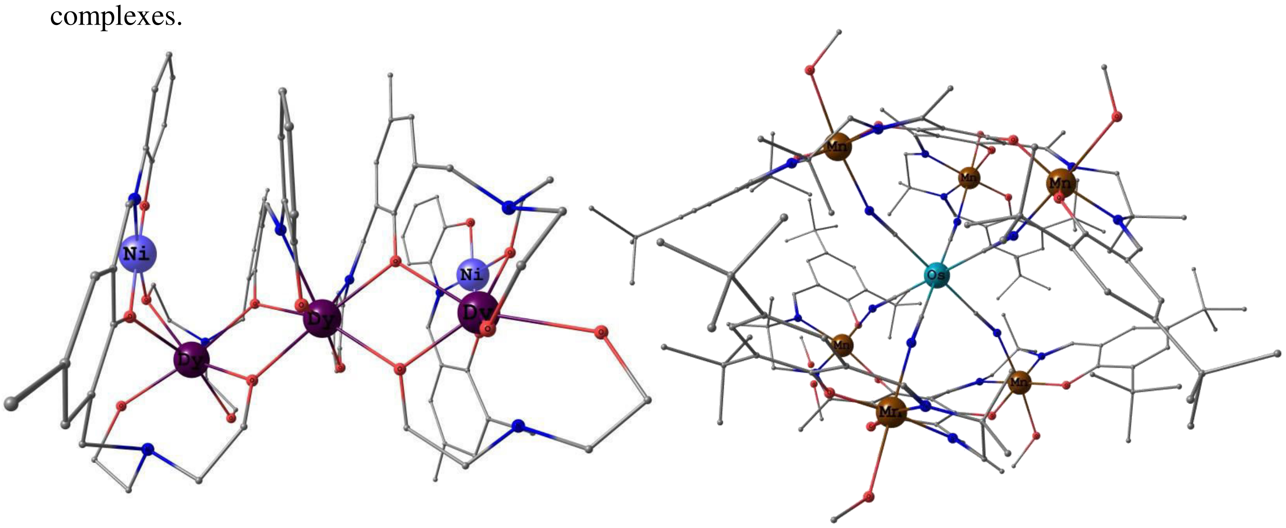

(a) (b)

Figure 27. Crystal structure of mixed SMMs (a) Ni2Dy3 [95] complex showing SMM behaviour with two relaxations. And (b) structure if $[Mn_6^{III}Os_{III}]^{3+}$ [96] SMM(a 3d-5d mixed SMM).

§1.1..1. 3d-3d[97] SMMs: These classes of compounds are not possible due to the difficulties encountered during their synthesis but still few exists. [39, 98]

§1.1.5.2. 3d-4d [99]SMMs: $K[(Me_3tacn)_6Mn^{II}Mo^{III}_6(CN)_{18}](ClO_4)_3$ cluster was the first initial example of a 3d-4d SMM which led to a D value of -0.33 cm^{-1} and energy barrier for reorientation of magnetization as 9.94 cm^{-1} . Three years after the inaugural example $\{Co^{II}_9[W^V(CN)_{8]6}.(MeOH)_{24}\}.]19H_2O$ was reported which exhibited effective barrier height of 19.3 cm^{-1}.

§1.1.5.3. 3d-5d[100, 101] SMMs(figure 27b)*:* Tetranuclear $(NBu_4)_4$ $[Ni\{ReCl_4(ox)\}_3]$ cluster was discovered in 2006 which remarkably possesses “star-like” structure and shows negative zero-field splitting of -0.46 cm^{-1} and SMM characteristics significant hysteresis loop. SMM characteristics has been detected in another W(V) based cluster $\{[W^V(bpy)(CN)_6]_2[Mn^{III}(L)]_2\}.3H_2O$ with barrier height of 22.2 cm^{-1}.

§1.1.5.4. 3d-4f[99] SMMs: The first 3d–4f [102-132] SMMs were reported in 2004: $[CuLLn(hfac)_2]_2$ (Ln = Tb, Dy; H_3L = 1-(2-hydroxybenzamido)-2-(2-hydroxy-3- methoxy-benzylideneamino)-ethane) squares with the 3d and 4f metals in an alternated array reported by Matsumoto et al., and the $[Dy_6Mn_6(H_2shi)_4(Hshi)_2(shi)_{10(}MeOH)_{10}(H_2O)_2]$ (H_3shi = salicylhydroxamic acid) complex, reported by PecoraroIn 2011, Brooker, Powell, Chibotaru and co-workers reported the first example of a 3d-4f SMM prepared using a macrocyclic ligand, $[Zn^{II}_3Dy^{III}(L44)(NO_3)_3(MeOH)_3]\cdot4H_2O$. This was rapidly followed by the independent report, by Nabeshimaand co-workers, of a rare example of an erbium (III)-based SMM of a closely related macrocycle, $[Zn^{II}_3Er^{III}(L_{45})(OAc)(NO_3)_2(H_2O)_{1.5}(MeOH)_{0.5}]\cdot H_2O\cdot 3MeOH$. Recently, Long and Rinehart[61] proposed simple rules in order to exploit the lanthanides' single-ion anisotropy for designing 4f ion based SMMs. According to their theory, to maximize the anisotropy of oblate ions (Ce(III), Pr(III), Nd(III), Tb(III), Dy(III) and Ho(III)) the crystal field should be such that the ligand electrons are concentrated above and below the xy plane i.e. axial coordination mode is preferred. On the other hand, for prolate ions (Pm(III), Sm(III), Er(III), Tm(III) and Yb(III)) an equatorial coordination geometry is preferred. Many of the reported 4f SMMs follow this prediction, and it is particularly useful for mononuclear lanthanide SMMs (SIMs). This simple qualitative way of predicting SMM behaviour could also be used to ascertain whether a lanthanide ion in a 3d–4f complex will contribute strongly to the complex anisotropy, and thus, to the SMM properties of the 3d–4f species. However, this must only be considered in a very qualitative manner. Given the difficulties in factoring out all of the contributions to a polynuclear complex's magnetic anisotropy, the relationship between the ligand arrangement around the lanthanide ion in a 3d–4f polynuclear complex and the complex's axial anisotropy will not be as straightforward as with mononuclear lanthanide SMMs. Ideally, the most anisotropic 3d metals should be combined with the right lanthanide to obtain new SMMs: the anisotropy of the 3d–4f complex will be a combination of the single-ion anisotropies of all the paramagnetic metal centres involved. As with any polynuclear coordination complex, the synthesis of 3d–4f SMMs most often follows a procedure of serendipitous self-assembly, where researchers try to provide the best reaction conditions to obtain complexes that might be new examples of SMMs. This is why there is such a rich structural diversity of 3d–4f SMMs, as is the case for transition metal SMMs. Of course the counterpart is the lack of control in the structure and properties of the prepared complexes. In the last few years the targeted substitution of a 3d metal by a lanthanide ion in a known transition metal polynuclear complex has been successfully done. This method has led to the isolation of 3d–4f complexes, where the position of the lanthanide ion could be predicted at the synthesis step. The $[Mn_{21}DyO_{20}(OH)_2(^tBuCOO)_{20}(HCO_2)_4(NO_3)_3(H_2O)_7]$ complex in figure 28 left, reported by Christou and co-workers in 2011, also shows hysteresis of the magnetization up to 3 K and has a large energy barrier of 74 K. It is notable that the aforementioned complex with 74 K U_{eff} is the largest barrier height reported to date for any 3d-4f based SMMs. Besides, some of the reported 3d-4f complexes are found to show two relaxation time with two effective barrier height for magnetization reorientation i.e. $[Co^{III}_2Dy^{III}_2(OMe)_2(teaH)_2(Piv)_6]$ shows U_{eff} of 51 and 127 K as obtained from AC measurements. Apart from these, several complexes combining Tb(III)/Er(III)/Ho(III)/Sm(III) lanthanide ions with Fe(III)/Cr(III)/Mn(II)/Co(II) have been reported to be SMM with considerable effective energy barrier (U_{eff}) required to bring back the magnetized state to its equilibrium state.

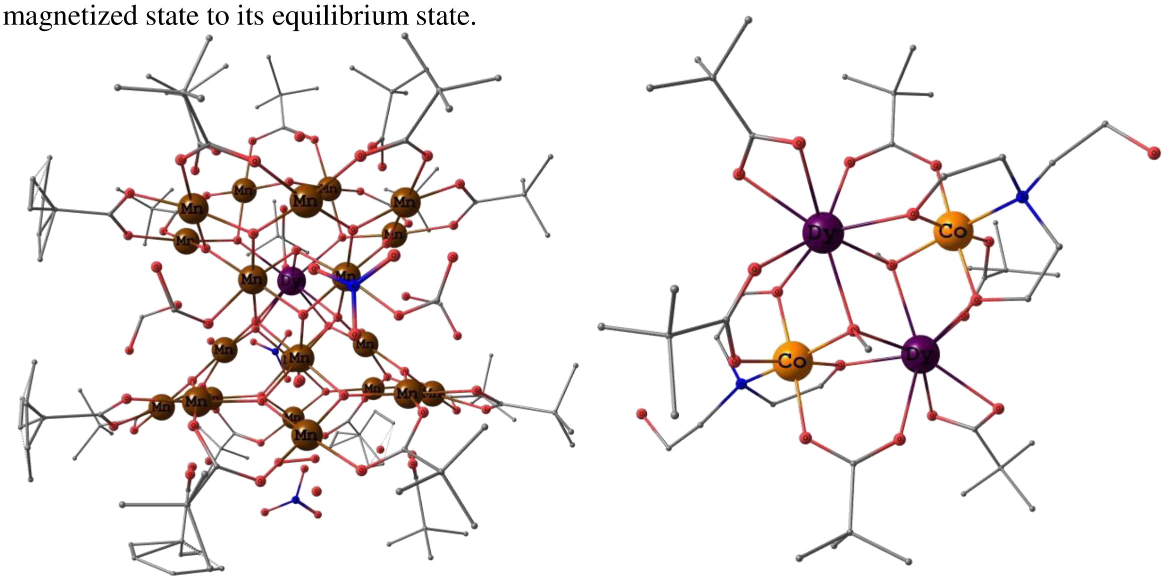

Figure 28. Crystal structures of some 3d–4f SMMs: left figure: $[Mn_{21}DyO_{20}(OH)_2(^tBuCOO)_{20}(HCO_2)_4(NO_3)_3(H_2O)_7]$ [133] and right one represent the structure: $[Co^{III}{}_2Dy^{III}{}_2(OMe)_2(teaH)_2(Piv)_6]$ [134]

The advances in the theoretical understanding of the magnetic properties of the lanthanide ions and their 3d–4f complexes are still lagging behind the advances in the synthesis of new complexes. There is still a lot to learn about heterometallic 3d–4f [135]complexes, especially about the magnetic coupling between 3d and 4f metals. We strongly believe the study of 3d– 4f interactions as it becomes more common, even in dinuclear model complexes, will provide good ideas for the design of new 3d–4f SMMs. From the knowledge base of 3d–4f SMMs reported up to 2014, dysprosium seems to be the best lanthanide to provide 3d–4f SMMs. Furthermore, two main trends of design of new 3d–4f SMMs have emerged as the most plausible to provide better 3d–4f SMMs in the near future: isolated lanthanide ions with a 3d metalloligand, as in the $[Mn_{21}Dy]$ reported by Christou and co-workers,38 with T_b = 3.0 K; or 3d–4f complexes with strong magnetic coupling between the metals to suppress QTM. Also a combination of these approaches emerges as a good option: a 3d–4f SMM with strong coupling between a unique lanthanide ion and a 3d metalloligand with large S that would help in quenching the QTM, thus increasing the blocking temperature.

§1.1.5.5. 4f-2p SMMs: In lanthanide SMMs, the large barriers are often attributable to single-ion behavior due to the weak coupling of lanthanide centers, thus limiting the further increase of ground quantum numbers, which seems to be a crucial roadblock to improve their anisotropy barriers and blocking temperature. Therefore, enhancing the exchange interactions between lanthanide centers has always been one of the most challenging tasks. Remarkably, the radical-bridged lanthanide (4f-2p) [136-138 139-143 144, 145 146-151] systems hold great promise in this respect. Labile and easily delocalized unpaired electron of radical facilitates fine tuning of intramolecular exchange interaction leading to

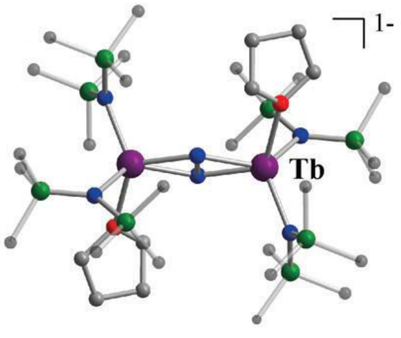

Figure 29. Crystal structure of $\{[(Me_3Si)_2N]_2(THF)Tb_2(\mu\text{-}\eta^2:\eta^2\text{-}N_2)]\}$

unprecedented magnetic properties and deeper understanding of the underlying magnetic properties. The first radical-bridged dinuclear lanthanide SMM was investigated by R. Sessoli and co-workers in 2007, where the nitronyl nitroxide radicals containing pyridine groups bridge two lanthanide ions and thus lead to obvious ferromagnetic interactions in the system. Particularly, the N_2^{3-} radical bridged lanthanide SMM still represents the hardest SMM magnet known to date, which exhibits the highest blocking temperature, $T_B = 14$ K[152] for complex $\{[(Me_3Si)_2N]_2(THF)Tb_2(\mu\text{-}\eta^2:\eta^2\text{-}N_2)]\}$: see Figure 29 and large coercive fields as a result of the extremely strong magnetic coupling. The fascinating results with these systems suggest the great ability of delocalized radical bridging ligands to propagate strong magnetic exchange coupling between lanthanide centers, and thus bring the goals of molecule-based information storage and processing closer to reality.

§1.2. Representative examples of Single Chain Magnets (SCMs):

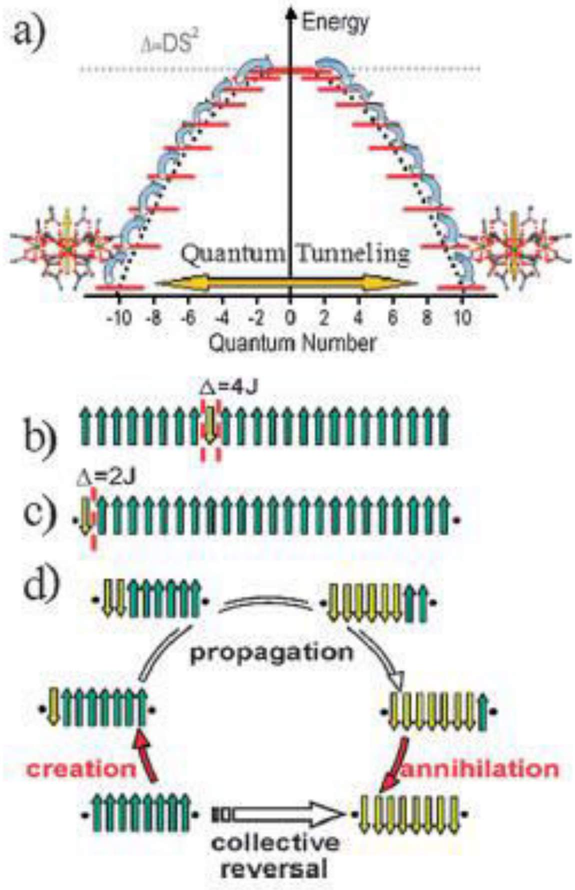

Figure 30. Mechanism for magnetization dynamics in SMMs and different relaxation mechanisms in SCMs. [7]

Single-Chain Magnets (SCMs) [111, 153 154-157 158 159, 160 161, 162 127, 144, 163 164, 165 7 166-168] are usually anisotropic single-spins or SMMs that are “stringed” into one-dimensional chains. They can be regarded as a special class of SMMs that are composed of magnetically isolated and individually magnetizable chains. Although it is well established that one-dimensional magnetic systems with short-range interactions do not experience long-range order at a finite temperature, the bulk material may remain in a paramagnetic state just as SMMs, and can also display long relaxation times of the magnetization promoted by the combination of a large uniaxial anisotropy and large magnetic interactions between the high-spin magnetic units of the chain. This type of one-dimensional system can thus behave as a magnet. Despite all the envisioned better-than-SMM properties of SCMs, successful examples of SCMs are still much fewer than SMMs, thus making the study of SCMs a field not only fundamentally stimulating but potentially rewarding with possibility of developing cutting-edge molecule based magnetic materials and corresponding technologies. In the adjacent figure 30 a) represents Double wall potential responsible for slow relaxation of magnetization in SMMs b) Glauber dynamics for an infinite chain c) GD for finite-size effects d) an alternative mechanism for short chains involving the collective reversal of all spins.

Although SMMs and SCMs have in common the blocking of the magnetization, which is associated to a large easy-axis magnetic anisotropy, the basic physics of SCMs is only partially similar to that of SMMs, and the competition with different mechanisms of slow relaxation of the magnetization, like spin glass behavior must always be checked. Both SCMs and SMMs require a strong easy-axis magnetic anisotropy and weak magnetic interactions but the physical mechanisms are quite different. In SMMs, the ground multiplet S is split in zero field in such a way that the two states with $M_S = \pm S$ lie lowest on each side of a double-well potential. To overcome the barrier $\Delta = DS^2$, generated solely by the magnetic anisotropy, the spin has to climb up all the other M_S states via spin–phonon interactions, following the extended Orbach process. The model behind the slow dynamics of SCMs is Glauber dynamics (GD), that was originally developed for 1D Ising ferromagnets and had found large application to different subjects before the advent of SCMs. The relaxation process begins with the reversal of one spin in the chain. An Ising system can only assume two orientations and this initial reversal will cost an energy $\Delta = -4J$ or $-4JS^2$, if spins different from unity are assumed, due to the magnetic exchange interactions J between two neighbouring spins. In SCMs, Δ depends on J and it is thus useful to produce chains with the highest possible intrachain coupling. The interesting link between SMMs and SCMs need to be further theoretically investigated as the 1D organization of interacting SMMs can instigate substantial enhancement of energy barrier for the reversal of magnetization. Due to the hysteresis, 0-D systems have been called single-molecule-magnets (SMMs) and 1D systems have analogously been called single-chain-magnets (SCMs), stressing the fact that the hysteresis arises from single-molecule or single-chain properties. This immediately implies that SMMs and SCMs can be made as small as the single constituent units without losing their magnetic properties.

Figure 31. Various synthetic approach for different SCMS.

In fact the conditions to be met to observe slow magnetic relaxation in 1D materials are rather stringent: 1) the ratio of the interaction within the chain, J, and that between chains, J', must be rather high, larger than 10^4 ; 2) the material must behave as a 1D Ising ferro- or ferrimagnet. First SCM property was detected in [Co(hfac)$_2$(NITPhOMe)],possesses 1D arrays with a helical structure which showed slow relaxation of magnetization and hysteresis effects.

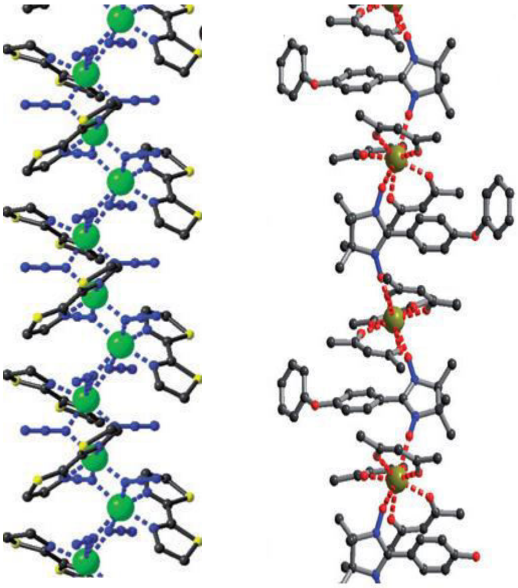

Figure 32. Chain structure of Co and Dy radical systems.

According to Glauber's theory, the origin of the slow magnetic relaxation was tracked to the large uniaxial type magnetic anisotropy, strong intrachain magnetic interaction, and negligible interchain interactions that hamper the transition to 3D magnetic ordering. Therefore, the synthetic approaches to build SCM include two respects: (i) to utilize appropriate bridging ligands as effective magnetic couplers to link uniaxial, anisotropic spin carriers, such as Co^{2+}, Ni^{2+}, Mn^{3+}, Fe^{2+} and lanthanide ions, into 1D chains and (ii) to use suitable diamagnetic separators so as to make these chains magnetically well isolated. In SCM literature, oxygen, cyano, oximate, azido, oxalato/oxamate, carboxylate, phosphate/ phosphinate and organic radical have been employed as bridging ligands because they can transport magnetic coupling efficiently. On the other hand, bulk co-ligands, long spacers, counter ions, etc., have been used for the purpose to reduce interchain interactions, and some co-ligands themselves also serve as intrachain bridges. The various combinations of intrachain bridges, metal ions, and separators have led to many SCMs with different spin structures. the first real homospin FO SCM, Co(bt)(N$_3$)$_2$ [169] (see Figure adjacent 164 left), was reported in 2003 which forms a 1D structure in which there are three independent octahedral Co sites, leading to a helical arrangement of the Co2+ metal ions along the chain. The versatility of NIT(R) radicals, has led to the rational design of the first rare-earth-based SCM [Dy(hfac)$_2$NIT(C$_6$H$_4$p-OPh)] (Fig. 32 right). While a transition to 3D order was observed in [Dy(hfac)$_2$NIT(C$_2$H$_5$)], it has been possible to suppress 3D ordering and obtain SCM behaviour by rationally introducing bulkier R = C$_6$H$_4$-OPh groups that suppress interchain magnetic interactions. Replacing the rare-earth-based SCMs the first family of isostructural SCMs, with tuneable anisotropy of the centres, has been created.

Although SCM have potential applications as memory devices and record media, their blocking temperatures are still too low at the moment. The first prospective goal in the synthesis of SCM is to raise the blocking temperature. The promising method to increase the blocking temperature is to enhance the intrachain coupling by choosing stronger magnetic intermediators.

§2. Characterisation of single molecule magnets:

The presence of zero-field splitting is a signature of magnetism in a quantum system. In non-magnetic quantum-dot systems, the absence of any zero-field splitting for Zeeman-split levels is observed universally (as required by Kramers' Theorem) for tunneling transitions from even (S = 0) to odd (S = 1/2) numbers of electrons. For odd-to-even transitions, only one spin transition is allowed for the lowest-energy tunneling transition because of Pauli blocking, but degeneracies at B = 0 are still generally observed for excited states. In quantum dots made from ferromagnetic nanoparticles, the presence of zero-field splitting has been observed previously due to magnetic anisotropy that affects tunneling transitions between states with $S \geq 1/2$. The presence of zero-field-split energy levels in four of our devices therefore demonstrates that tunneling in these devices is occurring via magnetic states with non-zero magnetic anisotropy.

Using SQUID (Superconducting Quantum Interference Device) magnetometry, it is possible to measure the magnetization of a sample with a defined mass in various applied fields (up to 7 T) and at various temperatures (as low as 1.8 K). This data may be fit to the Curie Law, or Curie-Weiss Law, to yield information about bulk and molar magnetic properties. In addition to applying a static magnetic field, it is also possible to measure the magnetic susceptibility in an alternating (ac) field which allows some insight into the dynamics of a magnetic system.

Graphic representations of the temperature dependence of χ, as well as M vs. H plots, are useful in identifying the magnetic character of a material. When measuring the magnetization as a function of temperature in a constant applied field, it is possible to calculate the molar magnetic susceptibility. Plots of χ vs. T are shown for a simple paramagnet (θ= 0 K), a ferromagnetically-coupled material (θ = 1 K), and an antiferromagnetically-coupled material (θ= -1 K). The plots are different based on their vertical asymptotes (dependent on θ), but the curves have the same shape which can be misleading. For that reason, it is more informative to plot χT vs T which gives clearer

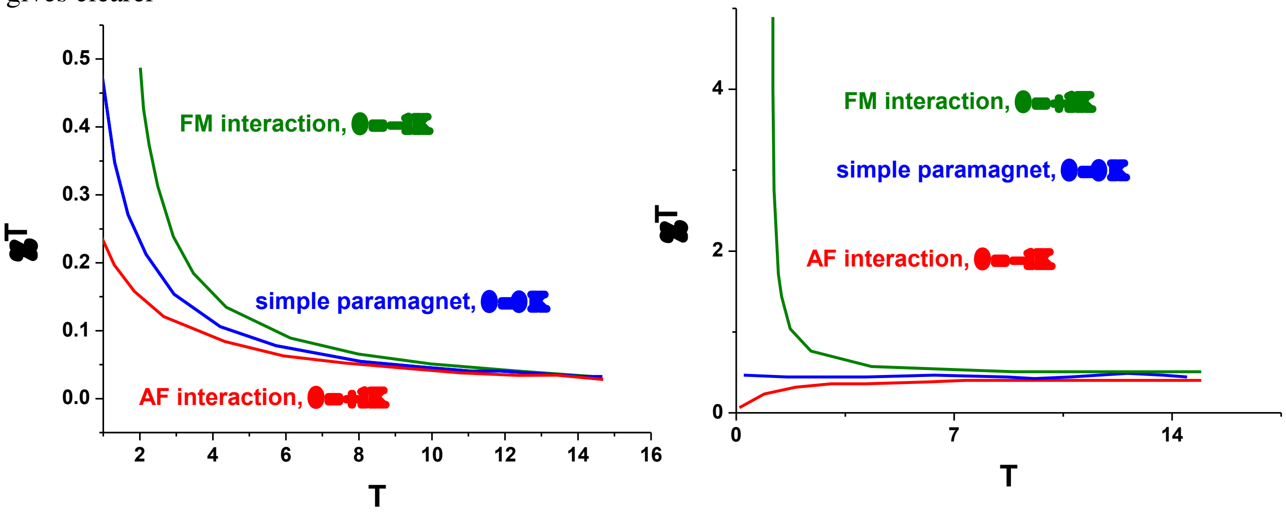

(a) (b)

Figure 33. a) implies plot of χ vs T for a simple paramagnet, ferromagnetic like material and an antiferromagnet material. b) represents of χT vs T for a simple paramagnet, ferromagnetic like material and an antiferromagnet material

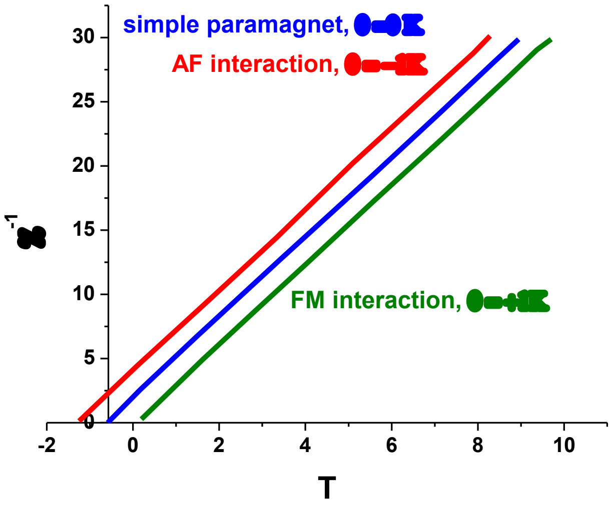

Figure 34. plot of χ^{-1} vs. T

evidence of the magnetic character. In this type of plot, the curve representing the ferromagnetically-coupled material curves up, the curve for the paramagnet is a horizontal line, and the curve for the antiferromagnetically - coupled material curves down. Example plots of χ^{-1} vs. T are also shown(adjacent figure 34). Notice that the paramagnet has $\theta = 0$ K and its x-intercept = 0 K, the ferromagnetically-coupled material has $\theta = 1$ K and its x-intercept = 1 K, and the same relationship applies for the antiferromagnetically-coupled material. The Curie constant, as stated earlier, can be determined from the slope of χ^{-1} vs. T which is C^{-1}.

As mentioned above, plots of M vs. H (constant temperature) are also useful in magnetic characterization. Curves for each type of magnetic material all have representative shapes which are generalized in adjacent figure 35. A characteristic of the curves for ferromagnets, paramagnets, and ferrimagnets is the saturation magnetization (M_s).

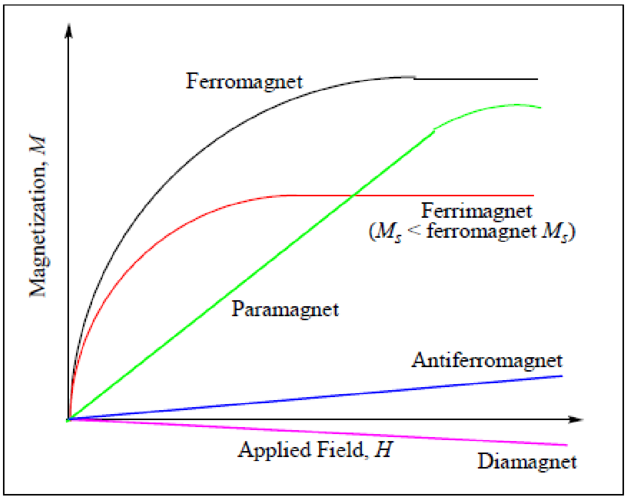

Figure 35. plot of magnetization vs magnetic field

This is the point where all of the magnetic moments in a material are aligned with the field, therefore the magnetization of the sample cannot increase any further. For a ferromagnet or paramagnet, the following equation stated earlier applies: $M_s = Ng\mu_B S$

In the above equation N is Avogadro's number, g is the Lande constant, S is the spin state and μ_B is the Bohr magneton. The saturation magnetization for a ferrimagnet can be expr- essed either of two ways depending on whether incomplete cancellation of the magnetic moments arises from differences in g or S, respectively:

$M_s = N \Delta g \, \mu_B S$ and $M_s = Ng \, \mu_B \, \Delta S$

In these equations, Δg refers to the difference in the Lande constant for the two spins of unequal magnitude and ΔS refers to the difference in spin.

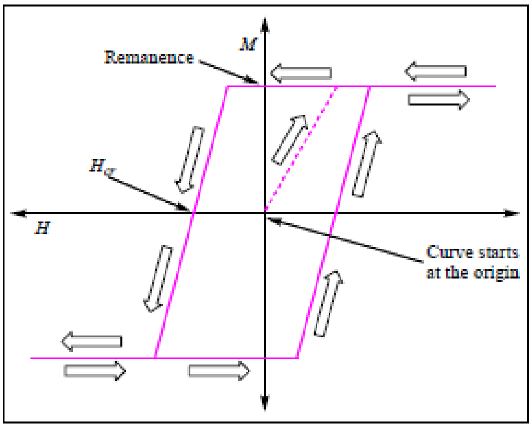

Figure 36. Pictorial representation of Magnetic hysteresis

Another important topic for M vs. H plots is the presence of hysteresis. This is a memory effect that can be observed when the magnetization curve does not follow the same path forwards and backwards as the applied field is cycled from positive to negative(adjacent figure 36 where M vs H plot shows hysteresis) . As the field is applied starting from zero field, the sample becomes magnetized (this segment of the curve is often omitted for clarity in the adjacent figure 36). As the field is lowered to zero, the sample retains some magnetization, which is referred to as the remanence. The sample remains magnetized until the applied field is strong enough in the negative direction to flip the spins; this field strength is referred to as the coercivity or coercive field (H_{cr}). The hysteresis loop is typically centered on the origin since the behavior of the magnetization as the field is reversed follows the same pattern.

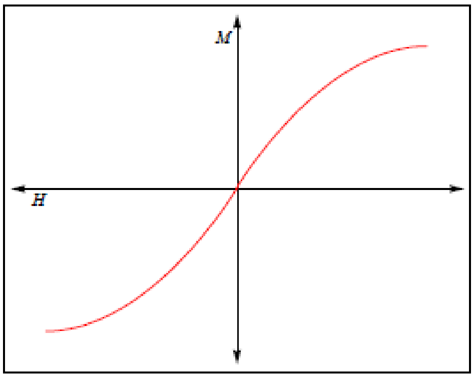

Figure 37. plot of magnetization vs magnetic field

Plots of M vs. H (below figure 37) also reveal whether the magnet in question is soft or hard. A soft magnet is magnetized when an external field is applied but it does not retain its magnetization when the applied field is removed. This translates into small values of coercivity and remanence. For an ideal soft magnet, the curve would follow the same path forwards and backwards as the applied field is oscillated as illustrated in adjacent figure. Hard magnets have large values of coercivity and remanence making them ideal for use as permanent magnets since they retain magnetization even when the applied field is removed. The curve in above figure 37 is an example of a hard magnet, assuming it is on the same scale as the plot in adjacent figure.

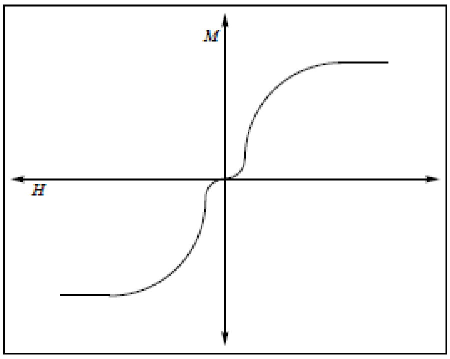

Figure 38. plot of magnetization vs magnetic field in a metamagnet

Metamagnetism is the presence of a field dependent phase transition from an antiferromagnetic to a ferromagnetic-like state. This can be illustrated by examining the adjacent M vs H (beside figure 38) plot for a metamagnet at low enough temperatures for spin interaction to be observed. The determining characteristic of this plot is the small slope of the curve around 0 G applied field which drastically increases at some field strength before levelling off in the stringer applied field. A small slope is indicative of antiferromagnetic interactions; the drastic increase in slope identifies the applied field strength at which ferromagnetic-like interactions take over.

The M vs. H data discussed up to this point has been based on a static (dc) magnetic field, where the magnetization at a given applied field is at thermal equilibrium. However, it requires a certain amount of time for a sample to adjust to any changes in the applied field. By using an alternating current (ac) to generate an alternating magnetic field, it is possible to measure the ac susceptibility, which gives some insight on the dynamics of a magnetic system.

The ac magnetic field, H_{ac}, can be described by the following equation:

$$H_{ac} = H_0 \cos(wt)$$

H_0 is the amplitude of the field, ω is the angular frequency ($\omega = 2\pi\nu$), and t is time. The magnetization of the sample, M_{ac}, lags behind H_{ac} since some time is required for the system to equilibrate. This can be written in the following terms:

$$M_{ac} = M_0 \cos(wt-\theta)$$

In the above equation, θ is the phase angle by which M_{ac} is shifted from the ac field. Using trigonometric relationships with the previous equations, the following can be written to describe the system:

$$M_{ac} = \chi' H_0 \cos(wt) + \chi'' H_0 \sin(wt)$$

$$\chi' = \frac{M_0}{H_0} \operatorname{Cos} \theta$$

$$\chi'' = \frac{M_0}{H_0} \operatorname{Sin} \theta$$

There are two expressions that make up the ac susceptibility, χ' and χ'', which can be defined with the following equation:

$$\chi_{ac} = \chi' + \chi''$$

The real component, χ' is the in-phase component which can be referred to as the dispersion since it describes the dispersive magnetic response of the sample to the applied ac field. The imaginary component, χ'' is the out-of-phase component which can be called the absorption since it refers to the energy absorbed by the system from the applied ac field. The characterisation of magnetic properties is greatly dependent on the measure of the ac susceptibility. Small ac field oscillates at a specific frequency of 1-1000 Hz

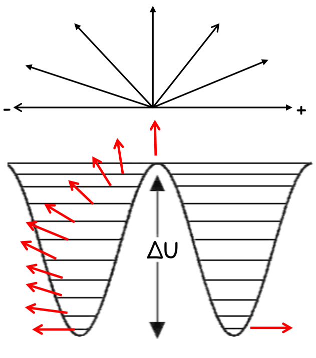

Figure 39. Impact of energy barrier for magnetization reversal on variations in magnetic field.

whose ability to follow the magnetic field relies on sweep rate and size of the energy barrier for reorientation of magnetization (figure 39).

The ac magnetic susceptibility can be used to determine the rate at which a SMM can convert from “spin up” to “spin down”. The ac field is oscillated at a set frequency. When this frequency equals the rate of magnetization reversal, a maximum in the out-of-phase ac susceptibility (χ_M'')is observed. At a given frequency of oscillation of the ac field, the temperature of a complex is varied to find a maximum in χ_M''.

There are several experimental manifestations of the fact that a molecule has a significant barrier for magnetization reversal and thus is functioning as a SMM at low temperatures: (i) there will be a divergence between the zero-field-cooled and field-cooled magnetization at some "blocking" temperature; (ii) perhaps the most classic indication is the observation of a hysteresis loop in the magnetization versus external magnetic field response; and (iii) there will be a frequency-dependent out-of-phase ac magnetic susceptibility signal because at low temperatures the magnetization of a single-molecule magnet will not be able to keep in phase with an oscillating magnetic field.

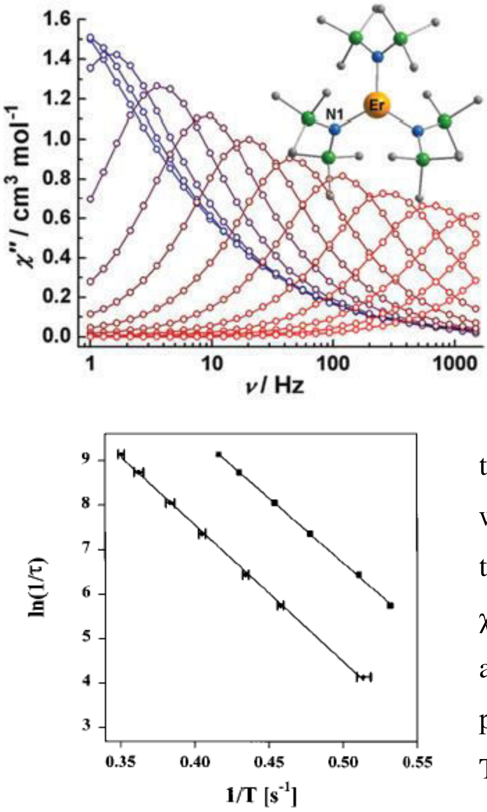

Figure 40. out-of-phase AC susceptibility for Er(III)-low coordinate complex and obtained data used to estimate U_{eff}.[5]

The ac susceptibility data were collected and maxima in χ_M'' vs temperature at particular frequency was noted. Such maxima values have been gathered for the χ_M'' vs temperature at different frequencies. Same maxima values were considered for χ_M'' vs frequency plot at specific temperature. These maxima values were also collected for χ_M'' vs frequency plot at different temperatures. This adjacent figure clearly implies the variation in the maximum point of the χ_M'' vs T plots which is dependent of frequency. This is an indicative of SMM characteristics in a three coordinate Er(III) complex shown inside the plot (figure 40). In relevance to this, we should mention that In SIMs magnetic properties are directly connected with the crystal field created by the surrounding ligands. This emphasizes the importance of crystal field environment in the design of novel SIMs. In SMMs coordination environment, number, local point group symmetry and ligand field strength all together need to be manipulated to obtain large energy barrier. Magnetic anisotropy in these SMMs arise due to interaction between single metal ion and the ligand field, resulting preferential orientation of the magnetic moment. This eventually generates a strong influence of coordination geometries on SIM properties. Thus, magnetic properties are affected not only by structural and electronic features of the molecule, but also by their surroundings resulting the spin dynamics method in SIMs a complex and poorly understood problem. Indeed, these processes can have significant influence on the field dependence of the relaxation time as well as field-induced multiple relaxation processes. Moreover, Lanthanide containing SIMs are attractive for testing synthetic design principles for slow paramagnetic relaxation because their properties can be tuned at will. In general, in a given crystal field, the ground magnetic state of the complex (characterized by the total angular momentum *J*), splits into $\pm M_J$ sublevels. In some instances, this leads to a J-splitting in which the levels with higher M_J values are stabilized with respect to the levels with lower M_J values. This leads to the appearance of a barrier between the M_J levels explaining superparamagnetic blocking in the SMMs. Hence, accurate crystal field around the lanthanide ion in order to stabilize the highest magnetic moment (M_S/M_J) of the respective ion and tuning the ligand field appropriately is an essential criteria to obtain improved SMM properties. Lanthanides prefer to have larger coordination number which brings forth distortion and destabilizes the desired orientation for the metal ion. Hence, lower coordination symmetry can be correlated to the higher symmetry which is expected to stabilize the preferred orientation. This has been proved by recent synthesis of low-coordinated improved SMMs(worthwhile to mention that, synthesis of low-coordinated molecule is cumbersome).

The aforestated χ_M'' vs T plots were used to determine the effective energy barrier (U_{eff}) of spin relaxation. Approximation of the resulting relaxation rate ($1/\tau$) versus T dependence(figure 78 in the adjacent figure) by the Arrhenius equation: $\tau=\tau_0 \exp(U_{eff}/kT)$, where τ is the relaxation time(can be procured from the T and frequency dependent out of phase magnetic susceptibilitydata), k is the Boltzmann constant, and τ_0 is the pre-exponential term, was done. The relaxation rates at a given temperature can be obtained from $\omega = 2\pi\nu = 1/\tau$ at the maxima of the χ_M'' peaks, where ν is the given oscillation frequency.

$$\frac{1}{\tau} = \frac{1}{\tau_0} \exp(-U_{eff} / KT)$$

$$\ln(1/\tau) = -U_{eff} / KT + \ln(1/\tau_0)$$

This is the characteristic behavior for a thermally activated Orbach process, where U_{eff} is the effective anisotropy energy barrier,k is the Boltzmann constant, and T is the temperature. A plot of ln ($1/\tau$) vs 1/T with data can be collected at various ac frequencies which may lead to adjacent figure in complexes with SMM characteristics. The least square fit to the above equation was expresses as a solid line in the ln ($1/\tau$) vs 1/T plot. Slope and intercept determines the effective barrier height for magnetization reorientation and relaxation time respectively.

§3. Prerequisites to design high temperature single molecule magnets:

To-date, Fine control over both the symmetry and nature of the ligand field is crucial in order to mitigate such perturbations and obtain improved SMM[28]s. Rinehart and Long proposed using the intrinsic anisotropic electron density distributions of the lanthanide ions in an extremely tangible electrostatic manner to design complexes that stabilize these large angular momentum states. The application of this strategy suggests that an axial ligand field is required for ions whose largest angular momentum states have oblate spheroid distributions, such as $\mathrm{Tb^{III}}$ and $\mathrm{Dy^{III}}$, while an equatorial field is required for those ions with prolate spheroid states, such as $\mathrm{Er^{III}}$ and $\mathrm{Yb^{III}}$. Designing a ligand field with the desirable charge distribution will be an effective approach to enhancing the axial anisotropy of the lanthanide center, given the potential of the electrostatic model in predicting the nature of single ion anisotropy for lanthanide ions. Elaborating a strongly uniaxial ligand field to force the magnetization reversal via higher excited energy levels seems to be a very promising route towards SMM with a high anisotropy barrier. The delocalized radical bridging ligands can provide an efficient magnetic exchange pathway between lanthanide ions, and thus the extension of such a system to other radical bridging ligands or larger lanthanide systems might hold great promise in achieving SMM with a higher blocking temperature. Hence, low coordinated, high symmetry complexes are the most suitable candidates to show large blocking temperature and suitable to prepare room temperature single molecule magnets. Complexes with such ligand field environment are supposed to show zero field SMM behaviour while distortion from idealised geometry induces perturbation. This leads to the fast zero-field QTM and suppression of SMM characteristics. On application of magnetic field, QTM can be reduced giving rise to the observation of field induced SMM behaviour owing to the large mixing of different m_J states.

§4. Synergy between experiment and theory:

Despite enormous synthetic effort expended in making novel examples of lanthanide-based SMMs, clear understanding of the origin of the slow relaxation of the magnetisation and the mechanisms of the Quantum Tunnelling of the Magnetisation (QTM) still remains scarce. Understanding the factors determining the formation of efficient barriers of blocking of magnetisation in SMMs is of primary importance for the fast advance of this new research area. Slow relaxation of magnetisation in SMMs can be achieved by effective involvement of anisotropy at the metal sites. Extensive studies on these SMMs based on lanthanides prove their importance due to their large spin-orbit coupling compared to the crystal-field splitting of the magnetic 4f-shell. All these studies have concluded the crucial participation of excited states of the lanthanide ions in the relaxation process of both mononuclear and polynuclear complexes. The anisotropy axis on the metal ions can be easily determined if the metal centers possess some symmetry elements. Using the angular overlap model, zero-field splitting and the direction of anisotropy axis can be estimated. However such qualitative ligand-field theories are extremely complex for lanthanides complexes rendering less accurate predictions. Although numerous experimental tools such as Inelastic Neutron scattering (INS), multifrequency high-field EPR, field and orientation dependent magnetic susceptibility have been used to investigate the magnetic anisotropy, none of them are suffice to resolve the directions of local anisotropy axes accurately. Here, we ("computational chemists") can find out the remedy using our computational tools. The only straightforward way to attain quantitative information about magnetic networks is via fragment quantum chemistry calculations taking into account the spin-orbit coupling non-perturbatively. Particularly, the direction of the local anisotropy axis on a metal site is easily gained as the main magnetic axis of the g tensors of the corresponding Kramers doublet. The single-ion properties of the 4f metal ions are difficult to depict due to the shielded nature of the 4f orbitals resulting weak exchange interactions. Recent advances in post Hartree-Fock multi-configurational *ab initio* methodology have made accurate quantum chemical calculations on paramagnetic 4f compounds possible. The Complete Active Space Self Consistent Field (CASSCF) method can accurately predict the magnetic properties of lanthanide complexes, and calculations of this type have become an indispensable tool for the explanation of increasingly interesting magnetic phenomena. Although CASSCF *ab initio* calculations are extremely versatile and implicitly include all the effects required to elucidate the magnetic properties, the results offer little in the way of chemically intuitive explanations and attainment of reliable results often requires considerable intervention by expert theorists equipped with access to powerful computational resources. In addition, the simple but amenable electrostatic model developed recently provides a crucial input for the theoretical modelling of the important single ion anisotropy requisite for blocking magnetic moments of lanthanide centers. Such a model can direct the chemical optimizations for better lanthanide SMMs operating at higher temperatures.

Normally, the magnetic anisotropy properties of SMMs are described by a spin Hamiltonian with the axial anisotropy parameter D and the transverse parameter E, and their corresponding higher-order anisotropy parameters B_n^k. However, the giant spin model breaks down when dealing with lanthanides. The magnetic properties of lanthanide ions are dominated by the internal nature of the f orbitals. Different from the 3d orbitals of transition metal ions in the ligand field and p orbital of radicals, f orbitals have strong unquenched orbital angular momentum and effective SOC. Owing to the SOC, the total angular momentum *J*, instead of the L and S, becomes the best quantum number. As a result, the giant spin model that is based on the spin operator cannot be used to analyse the magnetic properties of a system containing lanthanide.

To further our understanding of lanthanide-based molecular magnetism, the properties to be investigated require a very detailed study of the order as well as the separation of the low-lying f states, and subtle experimental techniques are required as well as the help of ligand field theory The splitting of the ground-state multiplet of a single lanthanide ion $^{2S+1}L_J$ can be described by the breaking of the spherical symmetry by the coordination field (also known as the ligand field). The resulting energies can be calculated by applying the irreducible tensor method, which is based on the idea that the effect of the ligands is modelled by a potential represented by the sum of the spherical harmonic operators, whose matrix elements can be calculated by the corresponding theory.

We and other computational chemists are using Gaussian, ORCA,MOLCAS[80, 92, 117, 157, 170-173 50, 80, 92, 117, 125, 157, 170-184]software in order to calculate the spin Hamiltonian parameters zero-field splitting, EPR spectroscopic parameters(g tensors), inter- and intra- molecular exchange interactions to corroborate experimental observations. Using computational tools we also have succeeded to gain deeper insights into the magnetization blockade , energy barrier and relaxation dynamics. We have also attempted to compare experimental magnetic susceptibility and magnetization data using our computed results which have been proved to be compatible for most of the complexes. All of our comparisons have been performed using experimentally synthesises crystal structures. Apart from these, we have modelled some of the structures to make predictions out of our calculations for promoting synthetic chemists towards preparing better SMMs.

§5. Conclusions:

Combining relevant and interesting physical properties in a controlled manner in the same material is an important topic for modern chemists. In particular, the engineering of new multifunctional materials associating magnetism with e.g. photo-activity, electro-activity, porosity, conductivity or other properties controlled by an external stimuli, are being currently targeted by many research groups. The prime benefits of SMMs over its other magnetic nanoparticles analogues are their monodispersive nature, similarity in the structure, and they can be derived directly from the crystal structure data, whose properties can be fine-tuned through the techniques of molecular chemistry. SMMs could be used for manufacturing of memory storage devices. Given the conditions to observe the quantum coherence are met, SMMs can be used for hardware for quantum computers. Requirement to synthesise large clusters with the aim to obtain improved SMM characteristics spur the quest of understanding different molecular properties in such large clusters. These enable such molecules to be ubiquitous and appealing for biocompatibility i.e.magnetic resonance imaging agent, magnetic drug delivery etc. Remarkably, a strong interest has been developed for looking at the design and the relaxation mechanism of lanthanide SMMs in the chemistry and physics communities, which is evident from the sheer number of research papers published and the ever expanding scope of the research. Many examples have indicated that lanthanide elements, especially Dy, display the superiority in magnetism over transition metal as a result of their ground states with highly anisotropic angular momentum. Therefore, the interest in lanthanide-based SMM is being continued with the goal of obtaining the SMM with higher effective barrier and blocking temperature, where the synthetic strategy should be the most crucial factor. It provides a tailored chemical environment (ligand field) to trap anisotropic ions and the alteration of the ligating groups available within the ligand to favor certain electronic states for the ion/aggregate will in turn influence the magnetic relaxation. The simplest strategy is to find the relation between the chemical environment of metal centers and the magnetic anisotropy of the compound/fragment, like the model developed by Long and coworkers, which could further give rise to effective targeting of new single molecule magnets with high anisotropy barriers. Inelastic neutron scattering and infrared spectroscopic investigations have allowed us to directly observe crystal field excitations within the ground Russell-Saunders multiplets.

Potentially, coordination chemistry provides the necessary tools for designing such new materials in rational and methodical approaches. However, the development of the preparative coordination chemistry is still behind the organic chemistry and consequently, it remains difficult for coordination chemists to design and synthesize, at will, polynuclear metal ion complexes or coordination polymers. Inspired from the protective groups in organic chemistry that direct the reactivity in particular positions, coordination chemists increase their structural control on the final material by using precursors with reduced degrees of freedom. Along this line, the used building-blocks are often carrying capping or strongly coordinating ligands to be able to direct the coordination properties and the final assemblies. Nevertheless, it is important to keep in mind that serendipitous self-assembly reactions have provided many systems of crucial importance to the development of the field of molecular magnetism and that the limitations of the modular approach with respect to structural design of polynuclear complexes are still important.

By creating complicated structures in a hierarchical fashion, the preparative coordination chemist can rely on an existing understanding of the first and second coordination sphere complexations and the well-understood relative robustness of coordination complexes.

Furthermore, this modular strategy offers an efficient transfer of the metal ion properties, imposed by the first coordination sphere, to extended structures. Thus, this approach allows us to control not only the spatial arrangements, but also the electronic structure of complicated systems. In this context, many combinations of metal ion modules and bridging ligands are unexplored to design new molecule-based magnetic materials including SMMs and related materials.

The ligand field vs oblate/prolate 4f electron density design ideais well illustrated by the dysprosium(III) bis(phthalocyanine) complexes. They are good SMMs in large part because the stronglyoblate (squashed like a hamburger pattie) character of the dysprosium(III) ion is enhanced by the provision of electron density from the two macrocycles above and below it (burger buns), in the axial sites, providing the energy minima (spin up and spin down along the easy axis), separated by the maximum energy wherethe spin passes through the hard plane which is orthogonal to the easy axis .These phthalocyanine complexes are good SMMs, but of course a simple analysis like this does not necessarilymean the U_{eff} will be high as there are a number of factors that influence SMM behaviour, including the possibility of QTM. Despite this caution, these general principles have moved researchers on from selecting terbium(III) and dys-prosium(III) simply because of the magnetic anisotropy conferred by strong spin–orbit coupling, to understanding how to exploit that anisotropy by careful ligand design, and indeed to use ligand design to also exploit the anisotropy particular to other, prolate, 4f ions.

It may be helpful to newcomers to the SMM field to point out that only two of the possible cases that favour slow relaxation of the magnetisation. Hence, when comparing the mixed 3d-4f monolanthanide SMMs with the purely 4f monometallic analogues, whilst there is a marked difference in the average value of Ueff, neither cate-gory of SMMs can be said to be more promising than the other with regard to practical applications, as all of them have extremely low $T_B$values (<8 K). Any applications of the best of the present SMMs would therefore require operation at below 8 K in order to obtain significant lifetimes over which the magnetisation is retained. Operation at such low temperatures is extremely expen-sive so precludes any widespread application of the present SMMs in devices (e.g. memory or quantum computing). To open up such applications, the blocking temperatures need to be considerablyimproved (preferably to liquid nitrogen temperatures or higher),and the lifetimes below T_B increased significantly too (preferably to the order of years). Whilst at present this seems a massive challenge, researchers in the superconductivity field faced a similarly challenging situation, and did make a huge step up in critical temperature, from liquid helium to liquid nitrogen temperatures, and superconducting materials are now used in a wide range of commercial applications.

Attempts to understand the slow magnetic relaxation in Kramers ions with positive axial anisotropy have outlined the importance of physical considerations beyond the symmetry around a 3d/4f ion, such as the importance of hyperfine interactions. Control of the relaxation pathways available to a single ion magnet should allow for improvement in performance as a potential data carrier. The physics of these compounds and how this relates to other possible applications for nanomagnets, such as quantum computing, still has wide scope for exploration. The chemical synthesis of these compounds presents a huge opportunity. If factors such as nuclear spin, symmetry around the metal ion, and modification of ligands are taken into account, then there are clearly a large number of experimental parameters to be tuned and explored.

So far, Single Molecule Magnets are a promising path to increase data density. The hurdle which still has to be overcome is to find a way of connecting the molecules to the macroscopic world. If this finally becomes possible, the benefit will be a thousand fold increase in density.

§21. References:

1. R. J. Blagg, L. Ungur, F. Tuna, J. Speak, P. Comar, D. Collison, W. Wernsdorfer, E. J. L. McInnes, L. F. Chibotaru and R. E. P. Winpenny, *Nat Chem*, 2013, **5**, 673-678.
2. C. R. Ganivet, B. Ballesteros, G. de la Torre, J. M. Clemente-Juan, E. Coronado and T. Torres, *Chem-Eur J*, 2013, **19**, 1457-1465.
3. K. R. Meihaus and J. R. Long, *J Am Chem Soc*, 2013, **135**, 17952-17957.
4. B. Barbara, L. Thomas, F. Lionti, I. Chiorescu and A. Sulpice, *Journal of Magnetism and Magnetic Materials*, 1999, **200**, 167-181.
5. P. Zhang, L. Zhang, C. Wang, S. Xue, S.-Y. Lin and J. Tang, *J Am Chem Soc*, 2014, **136**, 4484-4487.
6. S. K. Langley, D. P. Wielechowski, V. Vieru, N. F. Chilton, B. Moubaraki, L. F. Chibotaru and K. S. Murray, *Chemical Science*, 2014, **5**, 3246-3256.
7. L. Bogani, A. Vindigni, R. Sessoli and D. Gatteschi, *Journal of Materials Chemistry*, 2008, **18**, 4750-4758.
8. in *Magneto-structural correlations in exchange coupled systems*, eds. R. D. Willet, D. Gatteschi and O. Kahn, NATO Advanced Science Institute (ASI) series, Dordrecht,Netherlands:Reidel, 1985, vol. C140.
9. D. Bimberg, M. Grundmann and N. N. Ledenstov, in *Quantum Dot Heterostructures*, John Wiley & Sons Ltd., 1998.
10. N. N. Ledentsov, D. Litvinov, D. Gerthsen, G. A. Ljubas, V. V. Bolotov, B. R. Semyagin, V. A. Shchukin, I. P. Soshnikov, V. M. Ustinov and D. Bimberg, 2002.
11. W. Wernsdorfer, in *Advances in Chemical Physics*, John Wiley & Sons, Inc., 2001, pp. 99-190.
12. A. O. Caldeira and A. J. Leggett, *Physical Review Letters*, 1981, **46**, 211-214.
13. D. Gatteschi, A. Caneschi, L. Pardi and R. Sessoli, *Science*, 1994, **265**, 1054-1058.
14. R. S. D Gatteschi, J Villain, in *Molecular Nanomagnets*, Oxford University Press,Oxford, 2006.

15. A. J. Tasiopoulos, A. Vinslava, W. Wernsdorfer, K. A. Abboud and G. Christou, *Angewandte Chemie International Edition*, 2004, **43**, 2117-2121.
16. R. Sessoli, H. L. Tsai, A. R. Schake, S. Y. Wang, J. B. Vincent, K. Folting, D. Gatteschi, G. Christou and D. N. Hendrickson, *J Am Chem Soc*, 1993, **115**, 1804-1816.
17. L. Bogani and W. Wernsdorfer, *Nat Mater*, 2008, **7**, 179-186.
18. F. Cimpoesu, N. Dragoe, H. Ramanantoanina, W. Urland and C. Daul, *Physical Chemistry Chemical Physics*, 2014, **16**, 11337-11348.
19. J. Goura, J. Brambleby, P. Goddard and V. Chandrasekhar, *Chemistry – A European Journal*, 2015, **21**, 4926-4930.
20. Y.-L. Wang, B. Gu, Y. Ma, C. Xing, Q.-L. Wang, L.-C. Li, P. Cheng and D.-Z. Liao, *CrystEngComm*, 2014, **16**, 2283-2289.
21. P. Martín-Ramos, M. Ramos Silva, J. T. Coutinho, L. C. J. Pereira, P. Chamorro-Posada and J. Martín-Gil, *European Journal of Inorganic Chemistry*, 2014, **2014**, 511-517.
22. D. Zeng, M. Ren, S.-S. Bao, J.-S. Feng, L. Li and L.-M. Zheng, *Chemical Communications*, 2015, **51**, 2649-2652.
23. E. Colacio, J. Ruiz, E. Ruiz, E. Cremades, J. Krzystek, S. Carretta, J. Cano, T. Guidi, W. Wernsdorfer and E. K. Brechin, *Angewandte Chemie International Edition*, 2013, **52**, 9130-9134.
24. L. Ungur, J. J. Le Roy, I. Korobkov, M. Murugesu and L. F. Chibotaru, *Angewandte Chemie*, 2014, **53**, 4413-4417.
25. B. Na, X.-J. Zhang, W. Shi, Y.-Q. Zhang, B.-W. Wang, C. Gao, S. Gao and P. Cheng, *Chemistry – A European Journal*, 2014, **20**, 15975-15980.
26. S.-S. Liu, J. W. Ziller, Y.-Q. Zhang, B.-W. Wang, W. J. Evans and S. Gao, *Chemical Communications*, 2014, **50**, 11418-11420.
27. K. S. Pedersen, L. Ungur, M. Sigrist, A. Sundt, M. Schau-Magnussen, V. Vieru, H. Mutka, S. Rols, H. Weihe, O. Waldmann, L. F. Chibotaru, J. Bendix and J. Dreiser, *Chemical Science*, 2014, **5**, 1650-1660.
28. N. F. Chilton, *Inorganic Chemistry*, 2015, **54**, 2097-2099.
29. M. Evangelisti and E. K. Brechin, *Dalton Transactions*, 2010, **39**, 4672-4676.
30. J. R. Friedman and M. P. Sarachik, *Annu Rev Conden Ma P*, 2010, **1**, 109-128.
31. F. Neese and D. A. Pantazis, *Faraday Discuss*, 2011, **148**, 229-238.
32. P. Wang, S. Shannigrahi, N. L. Yakovlev and T. S. A. Hor, *Dalton Transactions*, 2014, **43**, 182-187.
33. D. E. Freedman, W. H. Harman, T. D. Harris, G. J. Long, C. J. Chang and J. R. Long, *J Am Chem Soc*, 2010, **132**, 1224-1225.
34. F. Neese and E. I. Solomon, *Inorganic Chemistry*, 1998, **37**, 6568-6582.
35. E. Colacio, J. Ruiz, A. J. Mota, M. A. Palacios, E. Cremades, E. Ruiz, F. J. White and E. K. Brechin, *Inorganic Chemistry*, 2012, **51**, 5857-5868.
36. S. D. Jiang, B. W. Wang, G. Su, Z. M. Wang and S. Gao, *Angew Chem Int Edit*, 2010, **49**, 7448-7451.
37. V. Mereacre, M. N. Akhtar, Y. Lan, A. M. Ako, R. Clérac, C. E. Anson and A. K. Powell, *Dalton Transactions*, 2010, **39**, 4918-4927.
38. D. P. Li, T. W. Wang, C. H. Li, D. S. Liu, Y. Z. Li and X. Z. You, *Chem Commun*, 2010, **46**, 2929-2931.
39. G. A. Craig and M. Murrie, *Chemical Society Reviews*, 2015, **44**, 2135-2147.
40. C.-M. Liu, D.-Q. Zhang, X. Hao and D.-B. Zhu, *Chemistry – An Asian Journal*, 2014, **9**, 1847-1853.
41. J. M. Zadrozny, D. J. Xiao, M. Atanasov, G. J. Long, F. Grandjean, F. Neese and J. R. Long, *Nat Chem*, 2013, **5**, 577-581.
42. H. Zhang, S.-Y. Lin, S. Xue, C. Wang and J. Tang, *Dalton Transactions*, 2014, **43**, 6262-6268.
43. D. Aravena and E. Ruiz, *Inorganic Chemistry*, 2013, **52**, 13770-13778.
44. F. Gao, M.-X. Yao, Y.-Y. Li, Y.-Z. Li, Y. Song and J.-L. Zuo, *Inorganic Chemistry*, 2013, **52**, 6407-6416.
45. N. F. Chilton, D. Collison, E. J. L. McInnes, R. E. P. Winpenny and A. Soncini, *Nat Commun*, 2013, **4**.
46. N. F. Chilton, S. K. Langley, B. Moubaraki, A. Soncini, S. R. Batten and K. S. Murray, *Chemical Science*, 2013, **4**, 1719-1730.
47. A. K. Mondal, S. Goswami and S. Konar, *Dalton Transactions*, 2015, **44**, 5086-5094.
48. C. Papatriantafyllopoulou, S. Zartilas, M. J. Manos, C. Pichon, R. Clerac and A. J. Tasiopoulos, *Chemical Communications*, 2014, **50**, 14873-14876.
49. J. J. Le Roy, I. Korobkov and M. Murugesu, *Chemical Communications*, 2014, **50**, 1602-1604.
50. A. Upadhyay, S. K. Singh, C. Das, R. Mondol, S. K. Langley, K. S. Murray, G. Rajaraman and M. Shanmugam, *Chemical Communications*, 2014, **50**, 8838-8841.
51. S. N. Konig, N. F. Chilton, C. Maichle-Mossmer, E. M. Pineda, T. Pugh, R. Anwander and R. A. Layfield, *Dalton Transactions*, 2014, **43**, 3035-3038.

52. S.-D. Jiang, B.-W. Wang and S. Gao, Springer Berlin Heidelberg, 2014, pp. 1-31.
53. D. N. Woodruff, R. E. Winpenny and R. A. Layfield, *Chemical reviews*, 2013, **113**, 5110-5148.
54. Z.-G. Wang, J. Lu, C.-Y. Gao, C. Wang, J.-L. Tian, W. Gu, X. Liu and S.-P. Yan, *Inorganic Chemistry Communications*, 2013, **27**, 127-130.
55. J. Vallejo, J. Cano, I. Castro, M. Julve, F. Lloret, O. Fabelo, L. Canadillas-Delgado and E. Pardo, *Chemical Communications*, 2012, **48**, 7726-7728.
56. A. Venugopal, F. Tuna, T. P. Spaniol, L. Ungur, L. F. Chibotaru, J. Okuda and R. A. Layfield, *Chemical Communications*, 2013, **49**, 901-903.
57. F. Tuna, C. A. Smith, M. Bodensteiner, L. Ungur, L. F. Chibotaru, E. J. L. McInnes, R. E. P. Winpenny, D. Collison and R. A. Layfield, *Angewandte Chemie International Edition*, 2012, **51**, 6976-6980.
58. G.-J. Chen, Y. Zhou, G.-X. Jin and Y.-B. Dong, *Dalton Transactions*, 2014, **43**, 16659-16665.
59. D.-K. Cao, R.-H. Wei, Y.-W. Gu, Y. Zhao and M. D. Ward, *RSC Advances*, 2014, **4**, 43064-43069.
60. G. Cucinotta, M. Perfetti, J. Luzon, M. Etienne, P. E. Car, A. Caneschi, G. Calvez, K. Bernot and R. Sessoli, *Angewandte Chemie*, 2012, **51**, 1606-1610.
61. J. D. Rinehart and J. R. Long, *Chemical Science*, 2011, **2**, 2078-2085.
62. P. I. Girginova, L. C. J. Pereira, J. T. Coutinho, I. C. Santos and M. Almeida, *Dalton Transactions*, 2014, **43**, 1897-1905.
63. M. Ren, D. Pinkowicz, M. Yoon, K. Kim, L. M. Zheng, B. K. Breedlove and M. Yamashita, *Inorganic Chemistry*, 2013, **52**, 8342-8348.
64. P.-H. Lin, I. Korobkov, W. Wernsdorfer, L. Ungur, L. F. Chibotaru and M. Murugesu, *European Journal of Inorganic Chemistry*, 2011, **2011**, 1535-1539.
65. M. Jeletic, P. H. Lin, J. J. Le Roy, I. Korobkov, S. I. Gorelsky and M. Murugesu, *J Am Chem Soc*, 2011, **133**, 19286-19289.
66. R. J. Blagg, C. A. Muryn, E. J. L. McInnes, F. Tuna and R. E. P. Winpenny, *Angew Chem Int Edit*, 2011, **50**, 6530-6533.
67. L. Chibotaru, Springer Berlin Heidelberg, 2014, pp. 1-45.
68. A. Watanabe, A. Yamashita, M. Nakano, T. Yamamura and T. Kajiwara, *Chemistry – A European Journal*, 2011, **17**, 7428-7432.
69. H. Wang, K. Qian, K. Wang, Y. Bian, J. Jiang and S. Gao, *Chemical Communications*, 2011, **47**, 9624-9626.
70. L. Sorace, C. Benelli and D. Gatteschi, *Chemical Society Reviews*, 2011, **40**, 3092-3104.
71. L. Ungur and L. F. Chibotaru, *Physical Chemistry Chemical Physics*, 2011, **13**, 20086-20090.
72. G. J. Chen, Y. N. Guo, J. L. Tian, J. Tang, W. Gu, X. Liu, S. P. Yan, P. Cheng and D. Z. Liao, *Chemistry*, 2012, **18**, 2484-2487.
73. Y. N. Guo, G. F. Xu, Y. Guo and J. K. Tang, *Dalton Transactions*, 2011, **40**, 9953-9963.
74. J. r. m. Long, F. Habib, P.-H. Lin, I. Korobkov, G. Enright, L. Ungur, W. Wernsdorfer, L. F. Chibotaru and M. Murugesu, *J Am Chem Soc*, 2011, **133**, 5319-5328.
75. Y. N. Guo, G. F. Xu, W. Wernsdorfer, L. Ungur, Y. Guo, J. K. Tang, H. J. Zhang, L. F. Chibotaru and A. K. Powell, *J Am Chem Soc*, 2011, **133**, 11948-11951.
76. F. Habib, P. H. Lin, J. Long, I. Korobkov, W. Wernsdorfer and M. Murugesu, *J Am Chem Soc*, 2011, **133**, 8830-8833.
77. G. Christou, D. Gatteschi, D. N. Hendrickson and R. Sessoli, *Mrs Bulletin*, 2000, **25**, 66-71.
78. N. Ishikawa, M. Sugita, T. Ishikawa, S. Koshihara and Y. Kaizu, *J Am Chem Soc*, 2003, **125**, 8694-8695.
79. N. Ishikawa, M. Sugita and W. Wernsdorfer, *Angew Chem Int Edit*, 2005, **44**, 2931-2935.
80. T. Rajeshkumar, S. K. Singh and G. Rajaraman, *Polyhedron*, 2013, **52**, 1299-1305.
81. M. del C. Fernández-Fernández, R. Bastida, A. Macías, P. Pérez-Lourido, C. Platas-Iglesias and L. Valencia, *Inorganic Chemistry*, 2006, **45**, 4484-4496.
82. M. T. Gamer, Y. Lan, P. W. Roesky, A. K. Powell and R. Clerac, *Inorganic Chemistry*, 2008, **47**, 6581-6583.
83. M. Gorlov, L. L. Hussami, A. Fischer and L. Kloo, *European Journal of Inorganic Chemistry*, 2008, **2008**, 5191-5195.
84. P. H. Lin, T. J. Burchell, R. Clerac and M. Murugesu, *Angew Chem Int Edit*, 2008, **47**, 8848-8851.
85. P. H. Lin, T. J. Burchell, L. Ungur, L. F. Chibotaru, W. Wernsdorfer and M. Murugesu, *Angew Chem Int Edit*, 2009, **48**, 9489-9492.
86. D. Savard, P. H. Lin, T. J. Burchell, I. Korobkov, W. Wernsdorfer, R. Clerac and M. Murugesu, *Inorganic Chemistry*, 2009, **48**, 11748-11754.
87. I. J. Hewitt, J. Tang, N. T. Madhu, C. E. Anson, Y. Lan, J. Luzon, M. Etienne, R. Sessoli and A. K. Powell, *Angew Chem Int Edit*, 2010, **49**, 6352-6356.

88. F. Luan, P. Yan, J. Zhu, T. Liu, X. Zou and G. Li, *Dalton Transactions*, 2015, **44**, 4046-4053.
89. S.-Y. Lin, C. Wang, L. Zhao, J. Wu and J. Tang, *Dalton Transactions*, 2015, **44**, 223-229.
90. W. Huang, J. J. Le Roy, S. I. Khan, L. Ungur, M. Murugesu and P. L. Diaconescu, *Inorganic Chemistry*, 2015, **54**, 2374-2382.
91. L. Ungur, S.-Y. Lin, J. Tang and L. F. Chibotaru, *Chemical Society Reviews*, 2014, **43**, 6894-6905.
92. G. Rajaraman, S. K. Singh, T. Gupta and M. Shanmugam, *Chemical Communications*, 2014, **50**, 15513-15516.
93. F. Pointillart, S. Golhen, O. Cador and L. Ouahab, *European Journal of Inorganic Chemistry*, 2014, **2014**, 4558-4563.
94. P. Zhang, Y. N. Guo and J. K. Tang, *Coordination Chemistry Reviews*, 2013, **257**, 1728-1763.
95. V. Chandrasekhar, P. Bag, W. Kroener, K. Gieb and P. Müller, *Inorganic Chemistry*, 2013, **52**, 13078-13086.
96. V. Hoeke, A. Stammler, H. Bögge, J. Schnack and T. Glaser, *Inorganic Chemistry*, 2014, **53**, 257-268.
97. R. Winpenny, G. AromÃ- and E. Brechin, in *Single-Molecule Magnets and Related Phenomena*, Springer Berlin Heidelberg, 2006, vol. 122, pp. 1-67.
98. S. M. J. Aubin, M. W. Wemple, D. M. Adams, H. L. Tsai, G. Christou and D. N. Hendrickson, *J Am Chem Soc*, 1996, **118**, 7746-7754.
99. M. Murugesu, A. Mishra, W. Wernsdorfer, K. A. Abboud and G. Christou, *Polyhedron*, 2006, **25**, 613-625.
100. J. P. Sutter, S. Dhers, R. Rajamani, S. Ramasesha, J. P. Costes, C. Duhayon and L. Vendier, *Inorganic Chemistry*, 2009, **48**, 5820-5828.
101. M. G. Alexandru, D. Visinescu, A. M. Madalan, F. Lloret, M. Julve and M. Andruh, *Inorg Chem*, 2012, **51**, 4906-4908.
102. S. Osa, T. Kido, N. Matsumoto, N. Re, A. Pochaba and J. Mrozinski, *J Am Chem Soc*, 2003, **126**, 420-421.
103. S. Osa, T. Kido, N. Matsumoto, N. Re, A. Pochaba and J. Mrozinski, *J Am Chem Soc*, 2004, **126**, 420-421.
104. A. Mishra, W. Wernsdorfer, S. Parsons, G. Christou and E. K. Brechin, *Chem Commun*, 2005, 2086-2088.
105. V. Chandrasekhar, A. Chakraborty and E. C. Sanudo, *Dalton Transactions*, 2013, **42**, 13436-13443.
106. F. He, M. L. Tong and X. M. Chen, *Inorganic Chemistry*, 2005, **44**, 8285-8292.
107. F. Mori, T. Ishida and T. Nogami, *Polyhedron*, 2005, **24**, 2588-2592.
108. T. Akitsu and Y. Einaga, *Polyhedron*, 2006, **25**, 2655-2662.
109. S. K. Langley, D. P. Wielechowski, V. Vieru, N. F. Chilton, B. Moubaraki, B. F. Abrahams, L. F. Chibotaru and K. S. Murray, *Angew Chem Int Edit*, 2013, **52**, 12014-12019.
110. K. Liu, W. Shi and P. Cheng, *Coordination Chemistry Reviews*, 2014, doi:10.1016/j.ccr.2014.1010.1004.
111. M. Zhu, Y. G. Li, Y. Ma, L. C. Li and D. Z. Liao, *Inorganic Chemistry*, 2013, **52**, 12326-12328.
112. C. Zhang, Y. Chen, H. Ma, T. Yu, B. Liu and H. Pang, *New Journal of Chemistry*, 2013, **37**, 1364-1370.
113. A. M. Madalan, K. Bernot, F. Pointillart, M. Andruh and A. Caneschi, *European Journal of Inorganic Chemistry*, 2007, 5533-5540.
114. F. Pointillart, K. Bernot, R. Sessoli and D. Gatteschi, *Chemistry – A European Journal*, 2007, **13**, 1602-1609.
115. M. Sarwar, A. M. Madalan, C. Tiseanu, G. Novitchi, C. Maxim, G. Marinescu, D. Luneau and M. Andruh, *New Journal of Chemistry*, 2013, **37**, 2280-2292.
116. L. Zhao, J. Wu, S. Xue and J. Tang, *Chemistry – An Asian Journal*, 2012, **7**, 2419-2423.
117. S. K. Singh, T. Rajeshkumar, V. Chandrasekhar and G. Rajaraman, *Polyhedron*, 2013, **66**, 81-86.
118. J. Cirera and E. Ruiz, *Comptes Rendus Chimie*, 2008, **11**, 1227-1234.
119. C. Lampropoulos, T. C. Stamatatos, K. A. Abboud and G. Christou, *Inorganic Chemistry*, 2008, **48**, 429-431.
120. J. B. Peng, Q. C. Zhang, X. J. Kong, Y. Z. Zheng, Y. P. Ren, L. S. Long, R. B. Huang, L. S. Zheng and Z. P. Zheng, *J Am Chem Soc*, 2012, **134**, 3314-3317.
121. E. Cremades, S. Gomez-Coca, D. Aravena, S. Alvarez and E. Ruiz, *J Am Chem Soc*, 2012, **134**, 10532-10542.
122. C. Lampropoulos, T. C. Stamatatos, K. A. Abboud and G. Christou, *Inorganic Chemistry*, 2009, **48**, 429-431.
123. V. Mereacre, A. M. Ako, R. Clerac, W. Wernsdorfer, I. J. Hewitt, C. E. Anson and A. K. Powell, *Chem-Eur J*, 2008, **14**, 3577-3584.

124. V. Chandrasekhar, B. M. Pandian, J. J. Vittal and R. CleÌ▯rac, *Inorganic Chemistry*, 2009, **48**, 1148-1157.
125. G. Rajaraman, F. Totti, A. Bencini, A. Caneschi, R. Sessoli and D. Gatteschi, *Dalton Transactions*, 2009, 3153-3161.
126. V. Baskar, K. Gopal, M. Helliwell, F. Tuna, W. Wernsdorfer and R. E. Winpenny, *Dalton Trans*, 2010, **39**, 4747-4750.
127. T. D. Pasatoiu, M. Etienne, A. M. Madalan, M. Andruh and R. Sessoli, *Dalton Transactions*, 2010, **39**, 4802-4808.
128. J. Rinck, G. Novitchi, W. Van den Heuvel, L. Ungur, Y. Lan, W. Wernsdorfer, C. E. Anson, L. F. Chibotaru and A. K. Powell, *Angewandte Chemie International Edition*, 2010, **49**, 7583-7587.
129. E. Colacio, J. Ruiz-Sanchez, F. J. White and E. K. Brechin, *Inorganic Chemistry*, 2011, **50**, 7268-7273.
130. G. Cosquer, F. Pointillart, Y. Le Gal, S. Golhen, O. Cador and L. Ouahab, *Chemistry – A European Journal*, 2011, **17**, 12502-12511.
131. J. Ferrando-Soria, E. Pardo, R. Ruiz-Garcia, J. Cano, F. Lloret, M. Julve, Y. Journaux, J. Pasan and C. Ruiz-Perez, *Chem-Eur J*, 2011, **17**, 2176-2188.
132. A. Helmstedt, N. Dohmeier, N. Müller, A. Gryzia, A. Brechling, U. Heinzmann, V. Hoeke, E. Krickemeyer, T. Glaser, P. Leicht, M. Fonin, T. Tietze, L. Joly and K. Kuepper, *Journal of Electron Spectroscopy and Related Phenomena*, 2015, **198**, 12-19.
133. C. Papatriantafyllopoulou, W. Wernsdorfer, K. A. Abboud and G. Christou, *Inorganic Chemistry*, 2011, **50**, 421-423.
134. L. Norel, M. Feng, K. Bernot, T. Roisnel, T. Guizouarn, K. Costuas and S. Rigaut, *Inorganic Chemistry*, 2014, **53**, 2361-2363.
135. L. Rosado Piquer and E. C. Sanudo, *Dalton Transactions*, 2015, **44**, 8771-8780.
136. Y.-L. Wang, Y.-Y. Gao, Y. Ma, Q.-L. Wang, L.-C. Li and D.-Z. Liao, *CrystEngComm*, 2012, **14**, 4706.
137. Y. Y. Gao, Y. L. Wang, P. Hu, M. F. Yang, Y. Ma, Q. L. Wang, L. C. Li and D. Z. Liao, *Inorganic Chemistry Communications*, 2013, **27**, 31-35.
138. X. L. Wang, *Inorganica Chimica Acta*, 2012, **387**, 20-24.
139. C. Wang, Y. L. Wang, Z. X. Qin, Y. Ma, Q. L. Wang, L. C. Li and D. Z. Liao, *Inorganic Chemistry Communications*, 2012, **20**, 112-116.
140. J. Lee, E. Lee, S. Kim, G. S. Bang, D. A. Shultz, R. D. Schmidt, M. D. E. Forbes and H. Lee, *Angewandte Chemie International Edition*, 2011, **50**, 4414-4418.
141. T. Ishida, R. Murakami, T. Kanetomo and H. Nojiri, *Polyhedron*, 2013, **66**, 183-187.
142. L. Bogani, *J Appl Phys*, 2011, **109**, 07B115-115.
143. C.-X. Zhang, X.-M. Qiao, Y.-K. Kong, B. Wang, Y.-Y. Zhang and Q.-L. Wang, *Journal of Molecular Structure*, 2015, **1081**, 348-354.
144. H.-L. Sun, Z.-M. Wang and S. Gao, *Coordination Chemistry Reviews*, 2010, **254**, 1081-1100.
145. R. N. Liu, Y. Ma, P. P. Yang, X. Y. Song, G. F. Xu, J. K. Tang, L. C. Li, D. Z. Liao and S. P. Yan, *Dalton Transactions*, 2010, **39**, 3321-3325.
146. F. Pointillart, Y. Le Gal, S. Golhen, O. Cador and L. Ouahab, *Chem Commun*, 2009, 3777-3779.
147. M. Zhu, X. Mei, Y. Ma, L. Li, D. Liao and J.-P. Sutter, *Chemical Communications*, 2014, **50**, 1906-1908.
148. C. Benelli, A. Caneschi, A. C. Fabretti, D. Gatteschi and L. Pardi, *Inorganic Chemistry*, 1990, **29**, 4153-4155.
149. C. Benelli, A. Caneschi, D. Gatteschi and L. Pardi, *Inorganic Chemistry*, 1992, **31**, 741-746.
150. C. Benelli, A. Caneschi, D. Gatteschi and R. Sessoli, *Inorganic Chemistry*, 1993, **32**, 4797-4801.
151. C. Benelli, A. Caneschi, D. Gatteschi and R. Sessoli, *Advanced Materials*, 1992, **4**, 504-505.
152. J. D. Rinehart, M. Fang, W. J. Evans and J. R. Long, *J Am Chem Soc*, 2011, **133**, 14236-14239.
153. D. Gatteschi and A. Vindigni, in *Molecular Magnets*, Springer Berlin Heidelberg, 2014, pp. pp 191-220.
154. W.-X. Zhang, T. Shiga, H. Miyasaka and M. Yamashita, *J Am Chem Soc*, 2012, **134**, 6908-6911.
155. P. Hu, C. Zhang, Y. Gao, Y. Li, Y. Ma, L. Li and D. Liao, *Inorganica Chimica Acta*, 2013, **398**, 136-140.
156. X. Chen, S. Q. Wu, A. L. Cui and H. Z. Kou, *Chem Commun (Camb)*, 2014, **50**, 2120-2122.
157. T. Rajeshkumar and G. Rajaraman, *Chem Commun*, 2012, **48**, 7856-7858.
158. R. Liu, P. Hu, L. Li, D. Liao and J.-P. Sutter, *Science China Chemistry*, 2012, **55**, 997-1003.
159. R. Liu, C. Zhang, X. Mei, P. Hu, H. Tian, L. Li, D. Liao and J.-P. Sutter, *New Journal of Chemistry*, 2012, **36**, 2088.
160. X. Feng, J. Liu, T. D. Harris, S. Hill and J. R. Long, *J Am Chem Soc*, 2012, **134**, 7521-7529.
161. M. Bałanda, Z. Tomkowicz, W. Haase and M. Rams, *Journal of Physics: Conference Series*, 2011, **303**, 012036.

162. N. Zhou, Y. Ma, C. Wang, G. F. Xu, J. K. Tang, S. P. Yan and D. Z. Liao, *Journal of Solid State Chemistry*, 2010, **183**, 927-932.
163. X. L. Wang, L. C. Li and D. Z. Liao, *Inorg Chem*, 2010, **49**, 4735-4737.
164. H. Miyasaka, M. Julve, M. Yamashita and R. Clerac, *Inorganic Chemistry*, 2009, **48**, 3420-3437.
165. T. C. Stamatatos, K. A. Abboud, W. Wernsdorfer and G. Christou, *Inorganic Chemistry*, 2008, **48**, 807-809.
166. C. Coulon, H. Miyasaka and R. Clerac, in *Single-Molecule Magnets and Related Phenomena*, Springer Berlin Heidelberg, 2006, vol. 122, pp. pp 163-206.
167. C. Benelli, A. Caneschi, D. Gatteschi, L. Pardi and P. Rey, *Inorganic Chemistry*, 1990, **29**, 4223-4228.
168. A. Caneschi, D. Gatteschi, N. Lalioti, C. Sangregorio, R. Sessoli, G. Venturi, A. Vindigni, A. Rettori, M. G. Pini and M. A. Novak, *Angew Chem Int Edit*, 2001, **40**, 1760-1763.
169. T.-F. Liu, D. Fu, S. Gao, Y.-Z. Zhang, H.-L. Sun, G. Su and Y.-J. Liu, *Journal of the American Chemical Society*, 2003, **125**, 13976-13977.
170. P. Christian, G. Rajaraman, A. Harrison, M. Helliwell, J. J. W. McDouall, J. Raftery and R. E. P. Winpenny, *Dalton Transactions*, 2004, 2550-2555.
171. S. K. Singh, N. K. Tibrewal and G. Rajaraman, *Dalton Transactions*, 2011, **40**, 10897-10906.
172. N. Berg, T. Rajeshkumar, S. M. Taylor, E. K. Brechin, G. Rajaraman and L. F. Jones, *Chem-Eur J*, 2012, **18**, 5906-5918.
173. J. Caballero-Jimenez, F. Habib, D. Ramirez-Rosales, R. Grande-Aztatzi, G. Merino, I. Korobkov, M. K. Singh, G. Rajaraman, Y. Reyes-Ortega and M. Murugesu, *Dalton Transactions*, 2015, **44**, 8649-8659.
174. F. K. Larsen, E. J. L. McInnes, H. El Mkami, J. Overgaard, S. Piligkos, G. Rajaraman, E. Rentschler, A. A. Smith, G. M. Smith, V. Boote, M. Jennings, G. A. Timco and R. E. P. Winpenny, *Angew Chem Int Edit*, 2003, **42**, 101-105.
175. G. Rajaraman, J. Cano, E. K. Brechin and E. J. L. McInnes, *Chem Commun*, 2004, 1476-1477.
176. G. Rajaraman, M. Murugesu, E. C. Sanudo, M. Soler, W. Wernsdorfer, M. Helliwell, C. Muryn, J. Raftery, S. J. Teat, G. Christou and E. K. Brechin, *J Am Chem Soc*, 2004, **126**, 15445-15457.
177. S. Piligkos, G. Rajaraman, M. Soler, N. Kirchner, J. van Slageren, R. Bircher, S. Parsons, H. U. Gudel, J. Kortus, W. Wernsdorfer, G. Christou and E. K. Brechin, *J Am Chem Soc*, 2005, **127**, 5572-5580.
178. M. L. Baker, G. A. Timco, S. Piligkos, J. S. Mathieson, H. Mutka, F. Tuna, P. Kozlowski, M. Antkowiak, T. Guidi, T. Gupta, H. Rath, R. J. Woolfson, G. Kamieniarz, R. G. Pritchard, H. Weihe, L. Cronin, G. Rajaraman, D. Collison, E. J. L. McInnes and R. E. P. Winpenny, *P Natl Acad Sci USA*, 2012, **109**, 19113-19118.
179. N. Berg, T. N. Hooper, J. J. Liu, C. C. Beedle, S. K. Singh, G. Rajaraman, S. Piligkos, S. Hill, E. K. Brechin and L. F. Jones, *Dalton Transactions*, 2013, **42**, 207-216.
180. S. K. Singh, K. S. Pedersen, M. Sigrist, C. A. Thuesen, M. Schau-Magnussen, H. Mutka, S. Piligkos, H. Weihe, G. Rajaraman and J. Bendix, *Chemical Communications*, 2013, **49**, 5583-5585.
181. S. K. Singh and G. Rajaraman, *Dalton Transactions*, 2013, **42**, 3623-3630.
182. T. Gupta and G. Rajaraman, *J. Chem. Sci.* , 2014, **126**, 1569-1579.
183. S. K. Singh, T. Gupta and G. Rajaraman, *Inorganic Chemistry*, 2014, **53**, 10835-10845.
184. C. Das, A. Upadhyay, S. Vaidya, S. K. Singh, G. Rajaraman and M. Shanmugam, *Chemical Communications*, 2015, **51**, 6137-6140.